BENCHMARK DESCRIPTION OF AN ADVANCED BURNER TEST REACTOR AND VERIFICATION OF COMET FOR WHOLE CORE CRITICALITY ANALYSIS IN FAST REACTORS

A Thesis
Presented to
The Academic Faculty

by

Richard Marion Ulmer III

In Partial Fulfillment
of the Requirements for the Degree
Master of Science in Nuclear Engineering in the
George W. Woodruff School of Mechanical Engineering

Georgia Institute of Technology
August 2014

BENCHMARK DESCRIPTION OF AN ADVANCED BURNER TEST REACTOR AND VERIFICATION OF COMET FOR WHOLE CORE CRITICALITY ANALYSIS IN FAST REACTORS.

Approved by:

Dr. Farzad Rahnema, Advisor
School of Mechanical Engineering
Georgia Institute of Technology

Dr. Bojan Petrovic
School of Mechanical Engineering
Georgia Institute of Technology

Dr. Anna Erickson
School of Mechanical Engineering
Georgia Institute of Technology

Date Approved: 5/5/2014

I dedicate this work to my loving wife, without whom I would not have had the drive to get this far. My parents, for their nurturing love and support that has allowed me to succeed. I also dedicate this to my brothers and the rest of my family, who have shaped me into what I am today.

ACKNOWLEDGEMENTS

I wish to thank my advisor Dr. Farzad Rahnema for his guidance on this work, as well as Dr. Bojan Petrovic and Dr. Anna Erickson for serving on my committee. I would also like to especially thank Kevin Connolly for a great deal of help throughout this process. Additionally, I would like to thank my wife and my parents for their support throughout everything I do. None of this would be possible without any one of you.

TABLE OF CONTENTS

LIST OF TABLES

LIST OF FIGURES

LIST OF SYMBOLS AND ABBREVIATIONS

ABTR	Advanced Burner Test Reactor
ARO	All Rods Out
NC	Near Critical
ARI	All Rods In
CR	Control Rod
IF	Inner Fuel
OF	Outer Fuel
TF	Test Fuel
RF	Reflector
RD	Relative Difference
RE	Relative Error
L1, L2, ..., L5	Active Core levels from 1 (lowest) to 5 (highest)
CE	Continuous Energy
15g	15 Group
RE	Relative Error
AVG	Average Absolute Relative Error
MRE	Mean Relative Error
RMS	Root Mean Square
$\sigma_{k\text{-}eff}$	Eigenvalue Uncertainty
σ_{pin}	Fuel Pin Uncertainty

SUMMARY

This work developed a stylized three dimensional benchmark problem based on Argonne National Laboratory's conceptual Advanced Burner Test Reactor design. This reactor is a sodium cooled fast reactor designed to burn recycled fuel to generate power while transmuting long term waste. The specification includes heterogeneity at both the assembly and core levels while the geometry and material compositions are both fully described. After developing the benchmark, 15 group cross sections were developed so that it could be used for transport code method verification. Using the aforementioned benchmark and 15 group cross sections, the Coarse-Mesh Transport Method (COMET) code was compared to Monte Carlo code MCNP5 (MCNP).

Results were generated for three separate core cases: control rods out, near critical, and control rods in. The cross section groups developed do not compare favorably to the continuous energy model; however, the primary goal of these cross sections is to provide a common set of approachable cross sections that are widely usable for numerical methods development benchmarking.

Eigenvalue comparison results for MCNP vs. COMET are strong, with two of the models within one standard deviation and the third model within one and a third standard deviation. The fission density results are highly accurate with a pin fission density average of less than 0.5% for each model.

CHAPTER 1

INTRODUCTION

When a new computational transport code is developed or a legacy code updated, a necessary first step is for that code to be thoroughly tested in a variety of scenarios in order to numerically verify the computational methods upon which it is constructed. While COMET has been benchmarked and proven against MCNP[8] for more traditional thermal systems, it has yet to be rigorously tested with a fast neutron design. In order to properly test a fast neutron spectrum, a large three dimensional full core model that is highly heterogeneous is required in order to represent a realistic reactor.

Typically, benchmark problems are kept as simple as possible by reducing the number of assemblies used and introducing significant levels of homogenization. This is typically a necessity, as transport methods become extremely complex and require a great deal of development before three dimensional heterogeneity is solvable. Recent improvements in solution methods, along with advancements in computational power, have allowed for the solving of problems that are significantly more complex. Whole-core benchmark problems without significant homogenization are not common, and this issue is dramatically compounded when fast neutron spectra are desired. The goal of this work is to develop an approachable, but fully defined and representative, full-core benchmark problem based on Argonne National Lab's conceptual Advanced Burner Test Reactor (ABTR), and then use that benchmark to verify COMET against MCNP. This reactor is a sodium cooled fast reactor designed to burn recycled transuranics with the goal of generating energy while transmuting long term radioactive waste. The reactor core model, as described by ANL, is included in Chapter 2 for the sake of completeness and to make this work as self contained as possible. In this design, a certain degree of geometric simplifications were necessary to decrease the complexity of the core. All such alterations were made with care to preserve the physics of the problem. The

simplifications, their justifications, and the stylized benchmark core configuration and specifications are covered in Chapter 3. Three configurations of the benchmark core were developed to test different scenarios: All Rods Out (ARO), All Rods In (ARI), and Near Critical (NC).

This particular reactor was used previously to benchmark MCNP against ERANOS by Allen et al.[3] However, that work was not intended as a benchmark description. Its primary goal was code benchmarking rather than the development of an approachable benchmark problem. As a consequence, it was not simplified, which results in a problem that is a more accurate representation of the core design but is unnecessarily burdensome from a methods development standpoint. This is not meant to be a full reference of all work on the subject of available benchmark problems; it is meant to be a useful contribution for developers and users in the form of a manageable fast reactor benchmark problem.

The benchmark specification contains a set of 15 group macroscopic material cross sections that are included to define a complete benchmark problem that can be readily used for numerical methods development. These cross sections sacrifice accuracy for ease of use because they are meant specifically for numerical methods development. As long as methods are being benchmarked and the same cross sections are used across the board, this is not an issue. Isotopic compositions are also provided to allow for continuous energy benchmarking and for the reader to generate their own cross sections should a higher degree of accuracy be desired. These cross sections are included in Appendix B, while the method used to generate them can be found in Chapter 4 alongside their energy bounds.

MCNP was used to compare the 15 group cross sections to the continuous energy cases with eigenvalues and pin fission density distributions in Chapter 5. Once cross sections were generated and the benchmark design finalized, COMET and MCNP were both run with the developed cross sections for direct method comparison. Those results

can be found in Chapter 6, where eigenvalues and pin fission densities are presented for each core case considered along with pin fission density peaking factors and control rod worth values. Finally, a runtime comparison between the two different codes will be presented before concluding remarks are presented in Chapter 7.

CHAPTER 2

CORE SPECIFICATION

This benchmark specification is composed of hexagonal assemblies, laid out in concentric rings around a central assembly. This layout is based on Argonne National Lab's 250 MWt ABTR design [1]. The overall design is very similar to the benchmark problem, but a number of simplifications and modifications were necessary. The intent of this benchmark is to create a computationally feasible version of the core that fully preserves the physics of the problem. Following is an outline of the core specifications as determined by Argonne. The simplified version will be covered in Chapter 3.

This chapter is included for the sake of completeness in an endeavor to make this document as self contained as possible. All Figures and Tables in this chapter come directly from Argonne[2] or are slightly modified versions thereof and thus will not be individually sited.

Radial Layout

The core is composed of 199 hexagonal assemblies placed in concentric rings, 60 of which are fuel assemblies. Reactivity control for normal operation, load following, and normal shutdown is handled by the uniform movement of the seven primary control rod assemblies. There are an additional 3 secondary control assemblies distributed throughout the inner core should there be issues with primary control. Other existing assembly types are: material test (filled with reflector in this case), reflector assemblies surrounding the active core, and finally, shield assemblies between the reflector and core barrel. The number and distribution of assemblies throughout the core is presented in Figure 1.

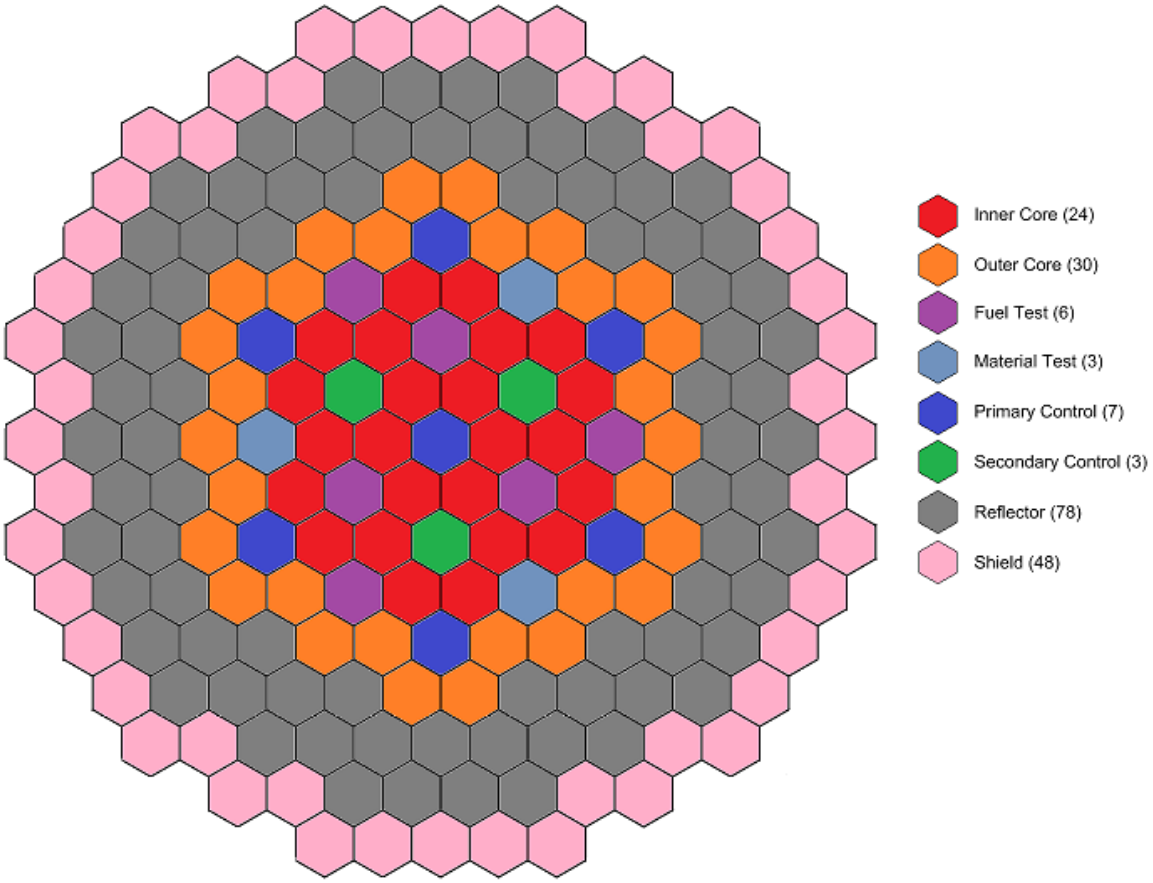

Figure 1. Map of Radial Core Distribution

Core dimensions have been expanded to account for the core's operating temperatures, which can be found in Table 1.

Table 1. Core Operating Temperatures

	Temperature (^{o}C)
Active core - Coolant - Structure - Fuel	 432.5 462.5 582.5
Reflector	432.5
Shield	355.0
Lower structure and reflector	355.0
Upper plenum and structure	510.0

Outside of the shield assemblies is a coolant channel, of varied size based on the positions of the different assemblies, which bridges the gap to the core barrel which has an inner diameter of 1.33 meters.

Axial Layout

The overall height of the core, after accounting for temperature effects on dimensions, is 341.66 cm. This height includes 50.24 cm of lower structural material and 30.15 cm of upper structural material, leaving 261.27 cm as the length of each assembly. Both the lower and upper structural sections of the core are homogenized because they are far too complex to be explicitly modeled. The upper structure specifically is a homogenized version of the fuel's lower reflector as that was deemed the best way to approximate the intricate structures above the core. The remaining 261.27 cm is highly dependent on the assembly of interest, as such it will be covered in the following assembly specifications section.

Assembly Geometric Specifications

There are 4 different assembly geometries based on the problem: fuel, control, reflector, and shield. There are three different fuel assemblies each with identical geometries. Primary and secondary control assemblies are geometrically and materially the same; they are simply treated separately because the secondary assemblies are not used during normal operation. In this case, the material test assemblies were specified to be the same as the reflector assemblies. The final assembly type is the shield, which forms the outermost ring of the core design.

Each assembly geometry is significantly different, the only real similarities being their hexagonal shape, length, and pitch simply by necessity of the core's overall geometry. All dimensions given have been thermally expanded.

Fuel Assembly

All three fuel assemblies have the same geometry; the only difference lies in the composition of the fuel inside the fuel pins. Each fuel assembly consists of 217 individual cylindrical fuel pins in a hexagonal matrix surrounded by a hexagonal structural duct. Each fuel pin is wire wrapped to maintain spacing; however this wire wrap has been homogenized into the fuel cladding. The fuel assemblies have four distinct regions: lower reflector, active core, expanded sodium bonds, and the gas plenum. The lower reflector is simply reflector material in place of the fuel slug within each pin cladding. The active core, as the name suggests, is where the fuel itself resides. The expanded sodium bonds are a segment above the active core where the thermal expansion of materials has also accounted for the expansion of the sodium bonds within the fuel. As these bonds expand, a portion of the bonding sodium is pushed above the active core into the gas plenum. Above the expanded sodium bonds lies the true gas plenum so that fission gas may remain contained within fuel pins. The parameters of the fuel assembly geometry, as supplied by Argonne, are given in Table 2.

Table 2. Fuel Assembly Parameters

Overall Length (cm)	341.663
Number of Pins	217
Fuel Pin Smear Density	75%
Fuel Pin Pitch (cm)	0.9134
Fuel Pin Total Radius (cm)	0.4024
Thickness of Cladding (cm)	0.0523
Fuel Pin Fuel Radius (cm)	0.3501
Fuel Pin Radius Including Wire Wrap (cm)	0.4057
Active Core Height (cm)	84.4108
Gas Plenum Height (cm)	120.5868
Length of Displaced Sodium Bond (cm)*	19.7637
Lower Reflector Height (cm)	60.293
Assembly Pitch (cm)	14.6850
Duct Outer Flat-Flat Distance (cm)	14.2826
Duct Thickness (cm)	0.3018

* This height is included within the gas plenum height.

A visual representation of the axial geometry of a fuel pin and the radial geometry of a fuel pin assembly is given below in Figure 2.

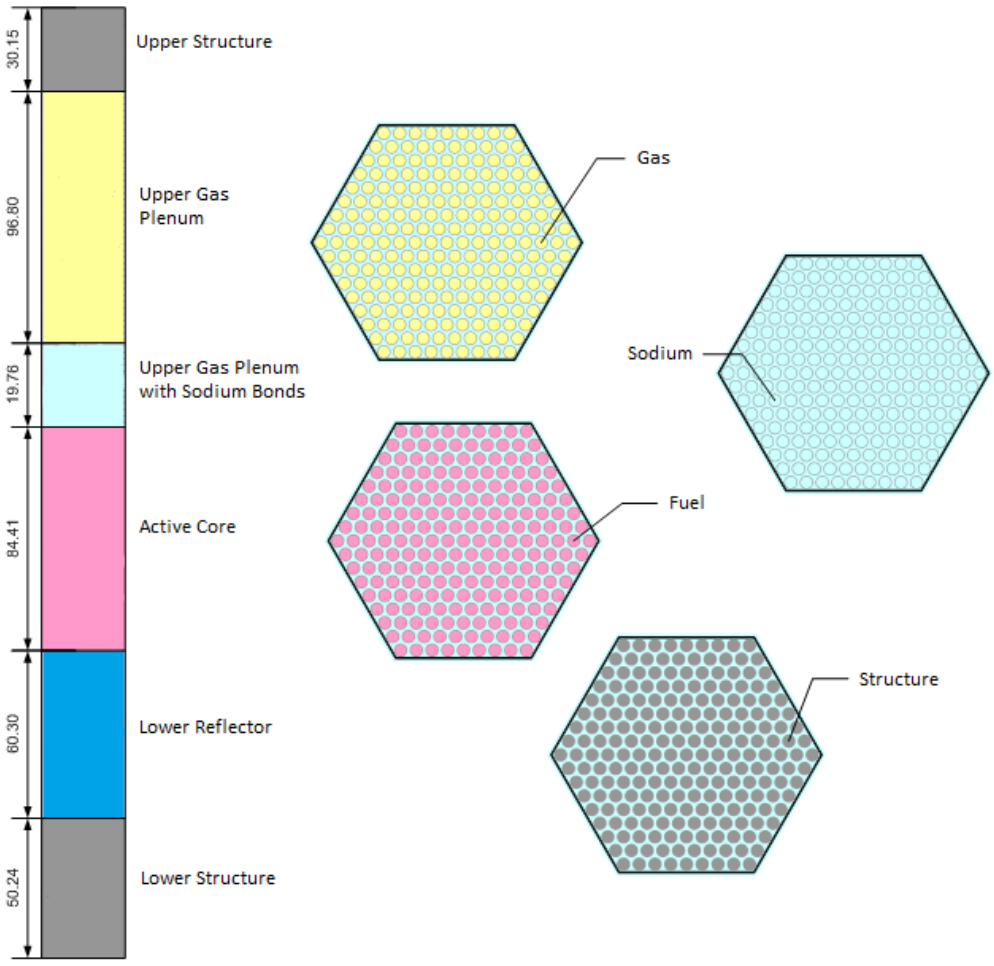

Figure 2. Fuel Assembly Geometry

Control Assembly

As previously mentioned, primary and secondary control assemblies are entirely identical. The difference lies in the design choice of secondary control being unused for normal operation. Control assemblies consist of 91 individual pins in a similar hexagonal matrix to the fuel assemblies and the pins are again wire wrapped to maintain proper spacing. There is a significant difference to the geometry of the assembly itself as an

inner duct is introduced between the control rods and the outer duct of the assembly. Between these two structural hexagons is an additional coolant channel. The control assemblies have five distinct regions: lower reflector, an empty segment, control rod follower, absorber, and the gas plenum. In this case, the lower reflector is a homogenized block of the fuel lower reflector so it consists of part structure and part sodium. The empty segment is exactly as it sounds, simply an empty channel of coolant where the control rods have been removed. The control rod follower is a cylinder with a diameter of 5.0 cm that immediately follows the absorber section of the control assembly. Above the follower is the absorber itself divided into the 91 pins. Finally, the gas plenum extends above the control rod absorber to the upper structure. The gas plenum occupies the same cladding as the absorber and is there to allow for gaseous products of absorption. Parameters for control assembly geometry follow in Table 3.

Table 3. Control Assembly Parameters

Overall Length (cm)	341.663
Number of Pins	91
Absorber Smear Density	85%
Absorber Pitch (cm)	1.2558
Absorber Total Radius (cm)	0.5585
Thickness of Cladding (cm)	0.0704
Absorber Radius (cm)	0.4881
Absorber Radius Including Wire Wrap (cm)	0.5626
Absorber Height (cm)	84.4157
Gas Plenum Height (cm)	31.14
Follower Radius (cm)	2.5149
Follower Height (cm)	16.8822
Empty Channel Height (cm)	85.51
Lower Reflector Height (cm)	42.32
Assembly Pitch (cm)	14.6850
Duct Outer Flat-Flat Distance (cm)	14.2826
Outer Duct Thickness (cm)	0.3018
Inner Duct Outer Flat-Flat Distance (cm)	12.8743
Inner Duct Thickness (cm)	0.3018

A visual representation of the geometry of a control rod assembly is below in Figure 3.

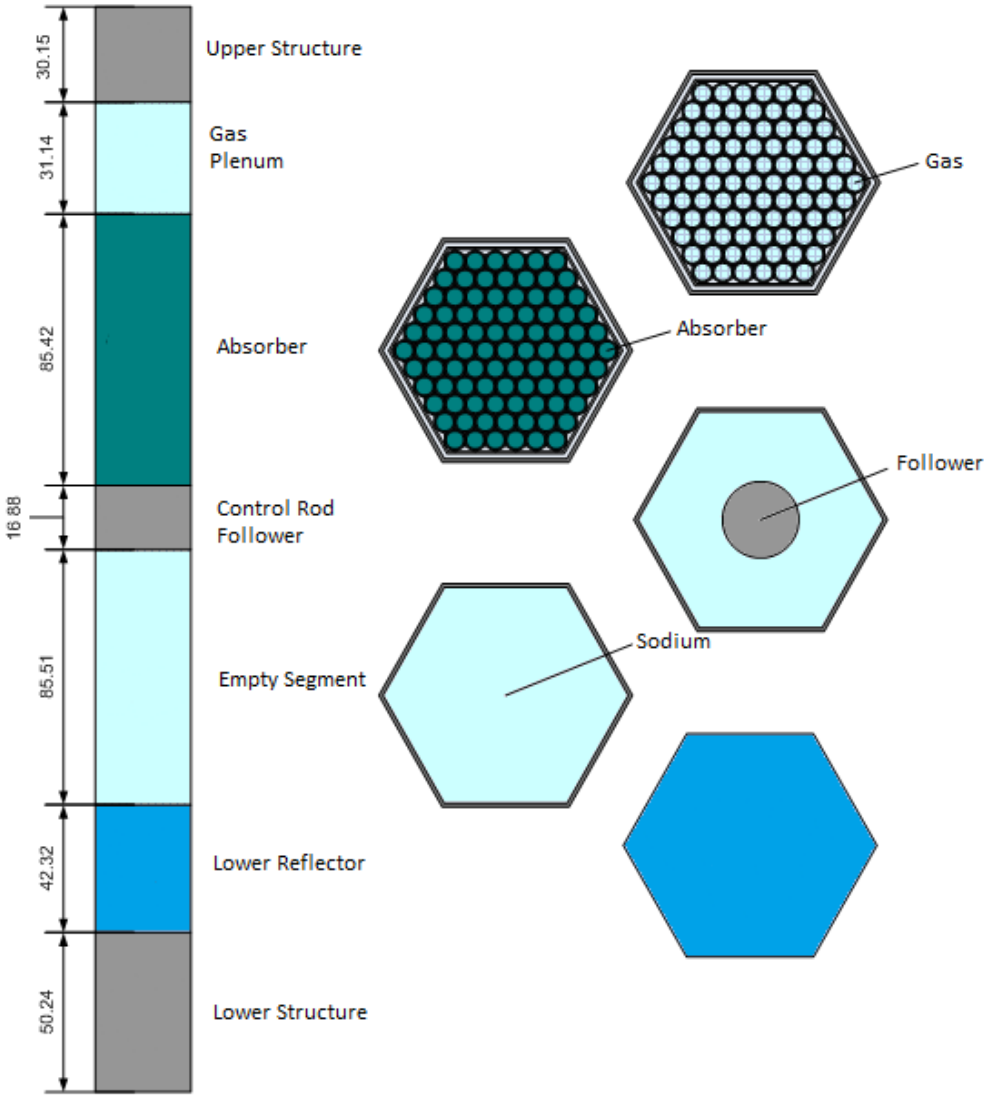

Figure 3. Control Rod Assembly Geometry

Reflector/Shield Assemblies

Reflector assemblies are far more simple than either the fuel or control rod assemblies. They consist of 91 pins in the familiar hexagonal arrangement for the entire extent of the core from the lower structure all the way up to the upper structure. They

lack the "inner duct" region that control rod assemblies have. Shield assemblies have the same overall geometry as the reflector assemblies, with the significant difference of only containing 19 pins. Parameters for both reflector and shield assemblies are included below in Tables 4 and 5. Following the tables is Figure 4, which contains the geometry of both reflector and shield assemblies.

Table 4. Reflector Assembly Parameters

Overall Length (cm)	341.663
Number of Pins	91
Pin Pitch (cm)	1.4151
Reflector Radius (cm)	0.7068
Reflector Rod Height (cm)	261.2714
Assembly Pitch (cm)	14.6850
Duct Outer Flat-Flat Distance (cm)	14.2826
Outer Duct Thickness (cm)	0.3018

Table 5. Shield Assembly Parameters

Overall Length (cm)	341.663
Number of Pins	19
Absorber Smear Density	81%
Shield Pin Pitch (cm)	3.0622
Absorber Total Radius (cm)	1.52035
Thickness of Cladding (cm)	0.2515
Absorber Radius (cm)	1.2789
Absorber Height (cm)	261.2714
Assembly Pitch (cm)	14.6850
Duct Outer Flat-Flat Distance (cm)	14.2826
Duct Thickness (cm)	0.3018

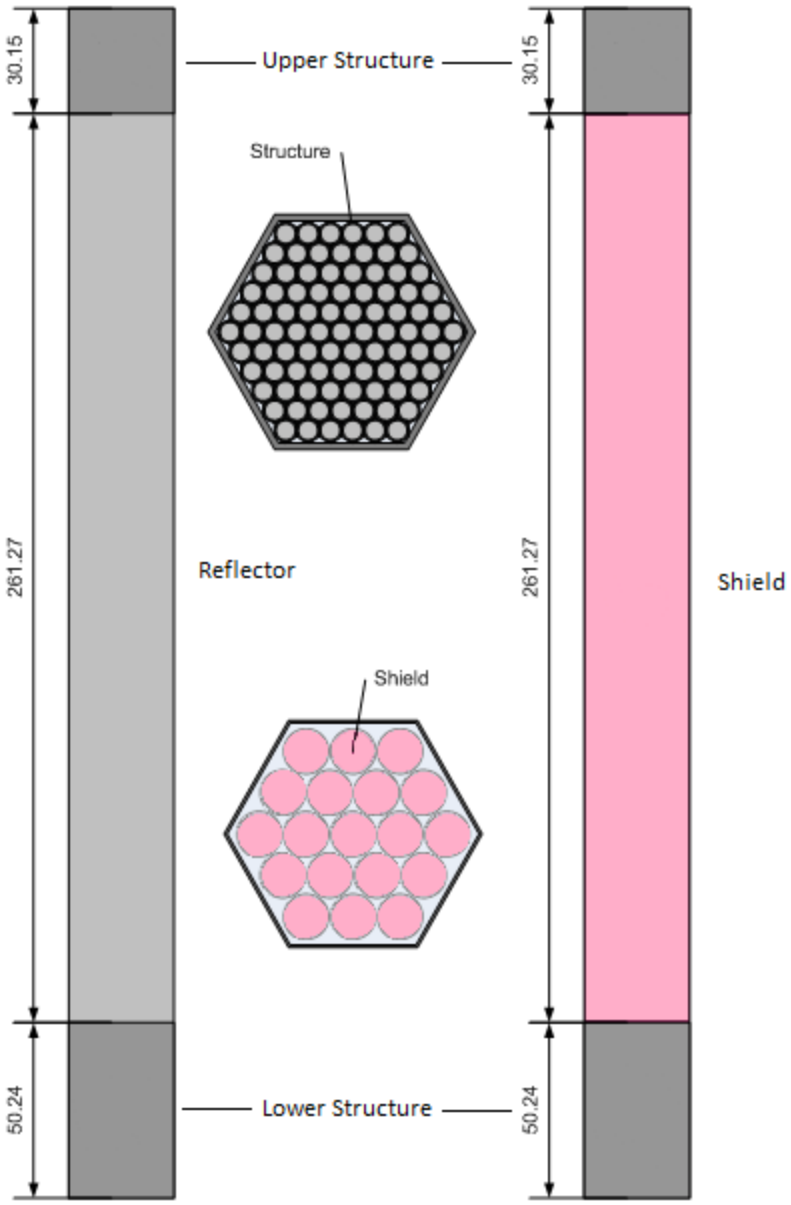

Figure 4. Reflector/Shield Assembly Geometry

Materials and Compositions

There are a total of 10 different materials used in the benchmark problem. A listing of these different material uses is supplied in Table 6 and actual material compositions are available in Appendix A. It should be noted that certain aspects of the

model "share" materials. For instance, the lower reflector region of a control rod assembly is the same as the overall core's upper structure.

Table 6. Benchmark Unique Materials

1) Inner Core Fuel
2) Test Site Fuel
3) Outer Core Fuel
4) Coolant (Sodium)
5) Structural Components and Reflector
6) Control Rod Absorber
7) Shield Absorber
8) Control Rod Follower & Core Barrel
9) Lower Structure
10) Upper Structure & Lower Reflector

CHAPTER 3

STYLIZED BENCHMARK SPECIFICATIONS

The development of a benchmark problem that retains the necessary physics to still be useful as a practical benchmark while simplifying the system enough to be reasonably evaluated is a challenge. The ABTR design is far too large and complex to explicitly model while still being accessible and manageable. Described in this section are the simplifications made to the reactor design previously presented for the sake of generating a reasonable benchmark problem.

Simplifications and Justifications

Following is a listing of all simplifications made and their justifications. Simplifications were made that retain the heterogeneity that is important for core physics but that simplify the core sufficiently to make it accessible. The primary goal of all simplifications is to preserve core physics while making the problem smaller and more manageable.

There are six different simplifications that were applied to the core to create the stylized benchmark problem: the shield assemblies at the edge of the core were removed, the material test assemblies were switched to test fuel (ANL had these defined as reflector assemblies), the control rod gas plenum was removed, the control rod follower was removed, the fuel gas plenum was removed, and last the axial dimensions of the core were shortened and standardized by removing outer material and adjusting dimensions. Some of these simplifications increased the multiplication factor while others decreased it. The end result of all of these simplifications was less than a 1% change in the value of k-effective.

As a brief note, it should be recognized that these simplifications are applied on top of any simplifications "baked into" the reactor design initially by ANL, such as the homogenized upper structure.

Shield Assemblies

Shield assemblies were removed from the problem entirely and replaced with an infinite absorber boundary condition. Their purpose is to minimize dose to and leakage from the reactor vessel. In order to cater to that purpose, the shield assemblies are borated. This boron absorber content, combined with the distance from the shielding to the active core along with the multiple reflector assemblies positioned inside of that shielding means that any neutrons reaching the shielding are unlikely to return. While this change ultimately does increase leakage to a small degree, the computational gains are significant. This simplification is one of the most significant computationally, instantly removing nearly 25% of assemblies in the model.

Material Test Assemblies

The material test assemblies were converted to test fuel assemblies where the original specification called for these assemblies to be reflector. This addition accounts for a 5% increase in the amount of fuel in the core, which clearly has a strong influence in the multiplication factor of the core. This is one of the most influential simplifications on k-effective, but also one of the most valuable. The original core configuration has no reflective symmetry, instead having one-third rotational symmetry. This change allows for the core to be modeled as one-sixth symmetric, dramatically improving the statistics.

Additionally, the other of the two most influential changes (axial shortening) works with this one to mutually cancel each other out.

Control Rod Gas Plenum

The control rod gas plenum was removed, and the control rod absorber was extended to the top of the problem in all cases (all rods in, all rods out, and near critical). This simplification served to decrease the complexity of the problem, and thus the number of unique structures that had to be modeled. Although this change is introducing additional absorber to the problem, the gas plenum was never inserted into the active core. Even in the ARI case, there was still absorber outside of the active core because the absorber height of the control rod is longer than the fuel height of the core. While this change does introduce additional absorber to the problem, it is a small change to the control rod outside of the active core.

Control Rod Follower

The control rod follower was removed and replaced by an empty channel of coolant. The follower served no purpose from a neutronics standpoint, and as seen in Figure 3, it takes up a small portion of the volume of the coolant channel below the control rod absorber.

Fuel Gas Plenum

The fuel gas plenum was replaced by extending the sodium bonds above the active core. This was done to remove another unique structure to simplify the complexity of the model. While this will decrease leakage, the gas plenum was already separated

from the active core by a portion of sodium bonds. This distance decreases the effect of this change. This change also helps compensate for some of the extra leakage introduced by the axial shortening of the core.

Axial Shortening and Dimension Standardization

The axial shortening of the problem was extensive. In total, the problem was reduced from a height of 341.663 cm to 151.92 cm. This simplification is the largest performed on the core, and introduces additional leakage in the axial directions.

The upper and lower structures were removed from the problem entirely. This accounts for 90.39 cm of the change and removes a unique material composition from the core as the lower structure's composition was not shared with any other portions of the core. Next, the lower reflector for fuel and control assemblies was shortened to 33.76 cm which removes 26.54 cm from the problem. Finally, the inactive region above the active core was shortened to 33.76 cm, accounting for the remaining 72.81 cm of change.

As previously mentioned, these changes have the impact of increasing the leakage of the system. However, the active core was not shortened and the changes made were performed from the outside in to minimize the impact they had. Ultimately, the height above and below the active core ended up being 33.76 cm. This is considered reasonable as the length between the radial edge of the active core to the radial edge of the problem is only 29.37 cm.

All axial dimensions of the core were adjusted slightly to be multiples of 16.88 cm. These adjustments were fractions of a cm. For instance, the active core was adjusted

from 84.41 cm to 84.4 cm. Other dimensions were taken to this standardization during the axial shortening process. This was the ideal length to separate the active core into 5 distinct regions of identical height for axial analysis. Standardized mesh sizes make modeling simpler in certain codes and was thus deemed appropriate since the changes could be made with negligible impacts to the core environment.

Stylized Radial Layout

Having covered the simplifications conceptually, the following sections visually review the layout of the core with the simplifications applied. Figure 5 shows the new radial layout of the core based on the alterations previously described.

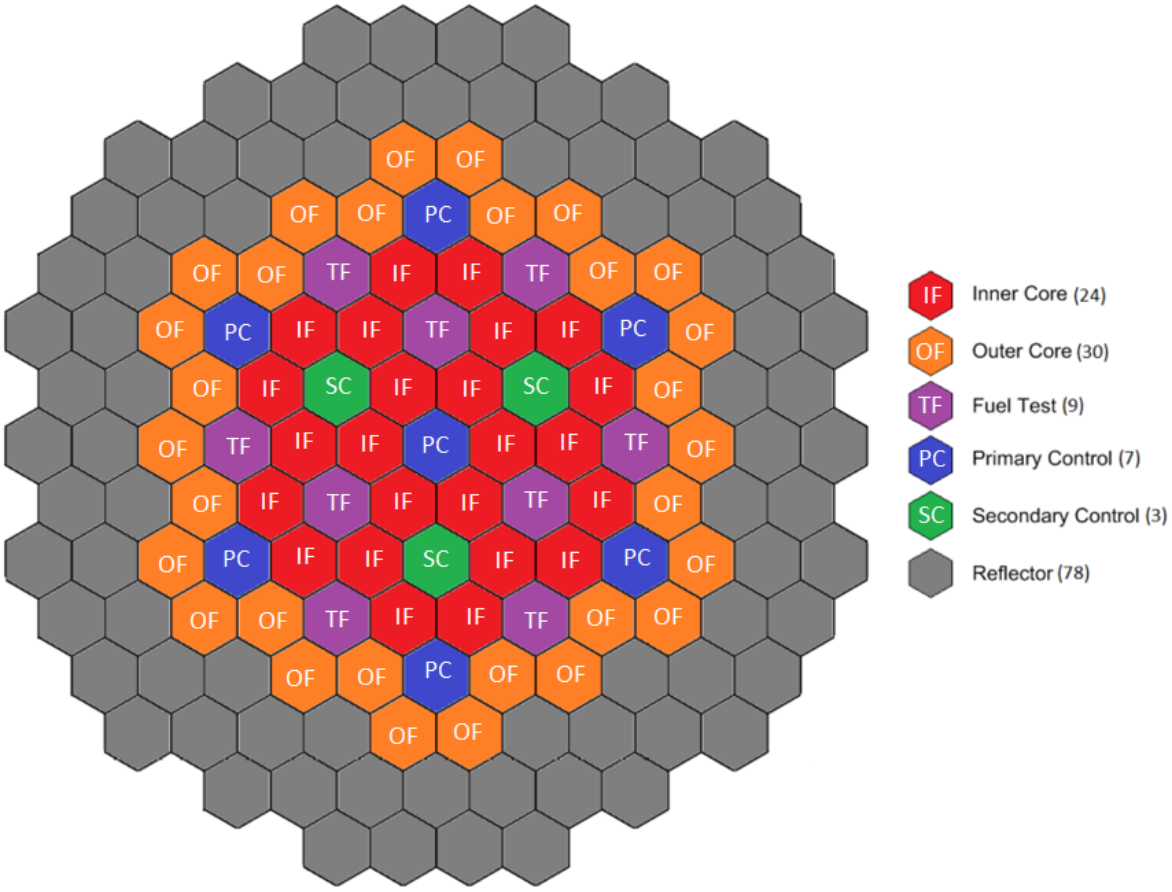

Figure 5. Radial Map of Simplified Core Geometry

Stylized Axial Layout

Where the previous section visually reviewed the radial layout of the core after simplification, this section will repeat the process for the axial layout of each unique assembly that is still present in the simplified core. Figures 6 through 8 display the benchmark layout. It should be noted that because the shield assemblies were removed, they have no representation here.

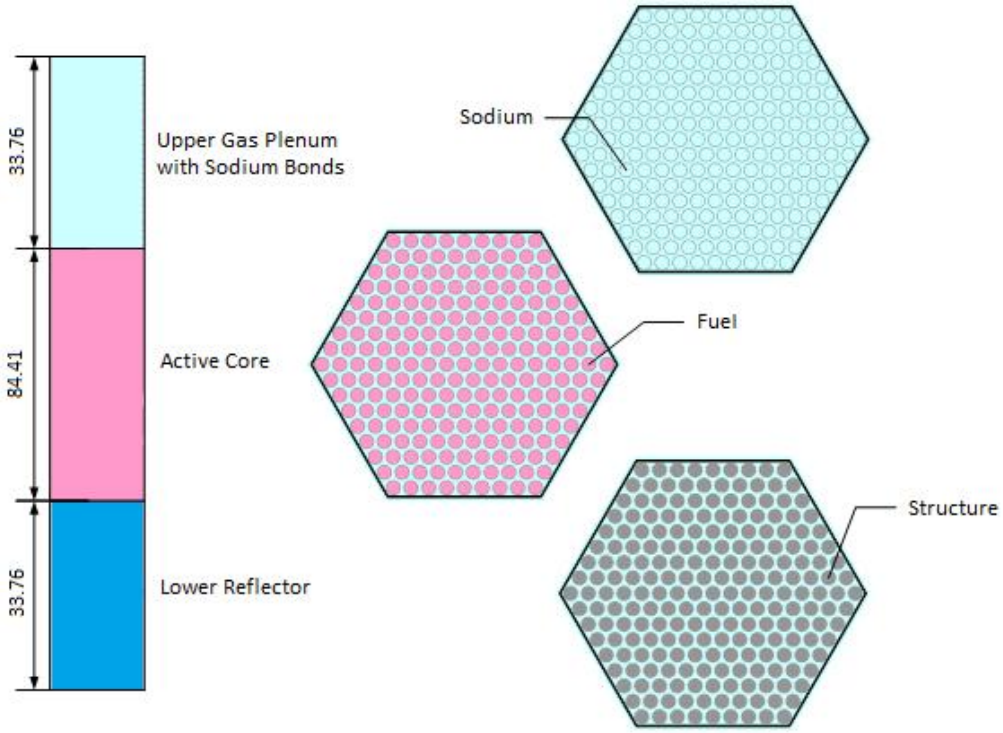

Figure 6. Benchmark Fuel Assembly Geometry

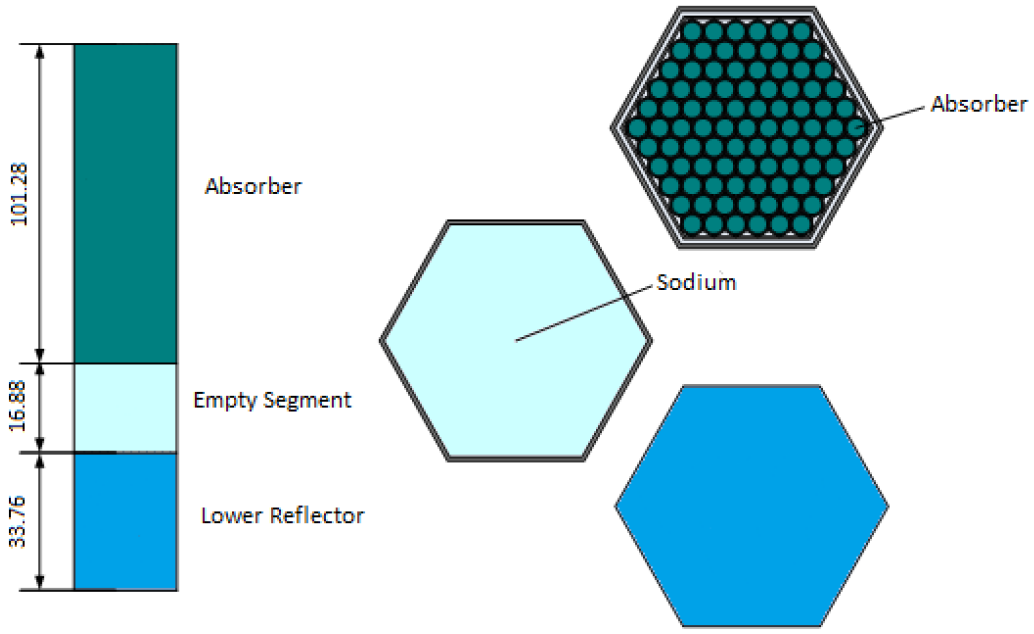

Figure 7. Benchmark Primary Control Rod Assembly Geometry (NC Case)

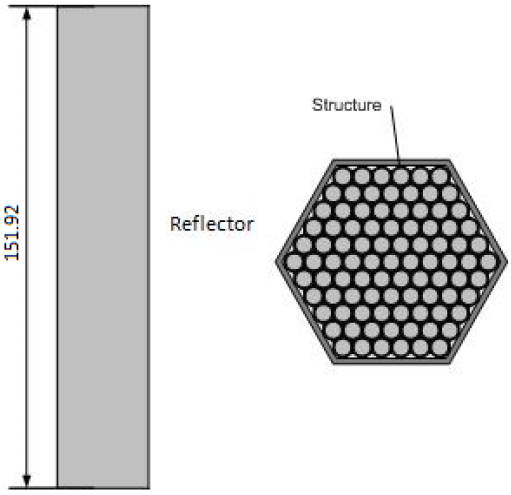

Figure 8. Benchmark Reflector Assembly Geometry

Stylized Assembly Specifications

The benchmark assembly parameters are supplied in Tables 7 through 9 with the updated dimensions after applying all simplifications. It should be noted that the control rod absorber length will have three different heights: withdrawn, partially inserted, and fully inserted corresponding to ARO, NC, and ARI core configurations respectively.

Table 7. Benchmark Fuel Assembly Parameters

Overall Length (cm)	151.92
Number of Pins	217°
Fuel Pin Smear Density	75%°
Fuel Pin Pitch (cm)	0.9134°
Fuel Pin Total Radius (cm)	0.4024°
Thickness of Cladding (cm)	0.0523°
Fuel Pin Fuel Radius (cm)	0.3501°
Fuel Pin Radius Including Wire Wrap (cm)	0.4057°
Active Core Height (cm)	84.4°
Length of Displaced Sodium Bond (cm)	33.76
Lower Reflector Height (cm)	33.76
Assembly Pitch (cm)	14.6850°
Duct Outer Flat-Flat Distance (cm)	14.2826°
Duct Thickness (cm)	0.3018°

° Quantities Unchanged from ANL Design

Table 8. Benchmark Control Assembly Parameters

Overall Length (cm)	151.92
Number of Pins	91°
Absorber Smear Density	85%°
Absorber Pitch (cm)	1.2558°
Absorber Total Radius (cm)	0.5585°
Thickness of Cladding (cm)	0.0704°
Absorber Radius (cm)	0.4881°
Absorber Radius Including Wire Wrap (cm)	0.5626°
Absorber Height ARO (cm)	33.76
Absorber Height NC (cm)	101.28*
Absorber Height ARI (cm)	118.16
Empty Channel Height (cm)	84.4**
Lower Reflector Height (cm)	33.76
Assembly Pitch (cm)	14.6850°
Duct Outer Flat-Flat Distance (cm)	14.2826°
Outer Duct Thickness (cm)	0.3018°
Inner Duct Outer Flat-Flat Distance (cm)	12.8743°
Inner Duct Thickness (cm)	0.3018°

° Quantities Unchanged from ANL Design

* This is for primary control, secondary is still withdrawn for the NC case.
** This is the maximum value, for any case other than ARO this value may shrink.

Table 9. Benchmark Reflector Assembly Parameters

Overall Length (cm)	151.92
Number of Pins	91°
Pin Pitch (cm)	1.4151°
Reflector Radius (cm)	0.7068°
Reflector Rod Height (cm)	151.92
Assembly Pitch (cm)	14.6850°
Duct Outer Flat-Flat Distance (cm)	14.2826°
Outer Duct Thickness (cm)	0.3018°

° Quantities Unchanged from ANL Design

Benchmark Core Configurations

The three core configurations that are described in this paper consist of: All Rods Out (ARO), Near Critical (NC), and All Rods In (ARI). The ARO case consists of all control banks fully withdraw from the active core. This leaves 33.76 cm of absorber that is the same height as the fuel assembly sodium bonds. The NC case has primary control inserted such that the top 67.52 cm of the active core is controlled while the secondary control rods remain withdrawn. Finally, the ARI case consists of both secondary and primary control fully inserted.

CHAPTER 4

CROSS SECTION LIBRARY GENERATION

Multi-group material cross sections were generated using the stochastic MCNP based MoCS-Gen code developed at Georgia Tech. MoCS-Gen generates multi-group libraries by generating fluxes through MCNP and then uses flux-weighting to collapse down to your target number of groups from continuous energy. A more in depth discussion of MoCS-Gen is outside the scope of this paper. Additional information is available from a paper by Pounders et al.[4]

The energy bounds of the 15 group structure were taken from a paper in which Aliberti et al.[5] explored various fast spectrum cross section groupings. The 15 group cross sections are presented in Appendix B.

Table 10. Cross Section Group Energy Bounds

Group	Upper Bound (MeV)
1	19.6
2	6.07
3	2.23
4	1.35
5	4.98E-1
6	1.83E-1
7	6.74E-2
8	2.48E-2
9	9.12E-3
10	2.04E-3
11	4.54E-4
12	2.26E-5
13	4.00E-6
14	5.40E-7
15	1.00E-7

Fast reactors pose a unique challenge when dealing with cross section generation because neighboring assemblies have a much larger influence on the flux shape inside an assembly. This is why the control can be confined to control assemblies instead of being dispersed throughout the core like in a PWR or BWR where the mean free path is much smaller. In order to compensate for this, cross sections were generated by modeling the entire core rather than single assemblies. This is where the advantage of MoCS-Gen had a significant impact. Instead of remodeling the entire core in another cross section generation code, which some are incapable of handling, it was possible simply to modify existing MCNP inputs with the tallies required by MoCS-Gen to save a significant amount of time and effort.

As previously stated, these cross sections were not selected to be as accurate as possible. They were selected to retain what accuracy was possible while focusing on ease of use. To that end, the scattering term was treated with linear anisotropy. While MoCS-Gen is capable of handling the required probability tables for higher order cross sections, this was considered an unnecessary burden for numerical methods benchmarking. Likewise, 33 energy groups would allow for a higher degree of accuracy but additional groups can complicate methods development. Finally, although operating temperatures are made available in this paper, the cross sections are room temperature. This was deemed appropriate as room temperature cross sections are readily available to users who may be testing with this benchmark problem. Should the reader desire more accurate cross sections, the isotopic compositions and operating temperatures are available elsewhere in this paper (Appendix A, Chapter 1 respectively).

CHAPTER 5

BENCHMARK REFERENCE SOLUTION

The benchmark problem for each configuration was modeled using continuous energy MCNP and 15 group libraries with an energy structure previously discussed. All fuel pins were modeled explicitly with full heterogeneity, and the only remaining homogenized structure in the core is the control rod lower reflector. This structure could not be modeled explicitly because core design information was supplied with it already homogenized. Models took advantage of the one-sixth symmetry of the core to improve statistics for a given number of particles.

Each model was run on 40 cores of a computer cluster with 320,000,000 neutron histories (160,000,000 for source convergence). An initial source convergence run was created by simulating 200,000 particles with 800 cycles. This converged source was then used with each model simulating 200,000 particles with 800 cycles (200 inactive) for the actual solution. The 84.4 cm tall active core was divided into regions of 16.88 cm for five distinct regions in which fission densities were tallied. These levels will be referred to as L1 - L5 where L1 is the lowest level (33.76 cm to 50.64 cm) and L5 the highest (101.28 cm to 118.16 cm). The core eigenvalues for all three configurations tested are found below in Table 11 for Continuous Energy (CE) vs. 15 group cross section libraries (15g) for MCNP. Also found in Table 11 is the difference between CE and 15g for each case, which will be given in per cent mille (pcm).

Table 11. Eigenvalues for Core Configurations and (Standard Deviation)

	ARO	NC	ARI
CE	1.04677 (.00005)	0.98290 (.00005)	0.92729 (.00005)
15g	1.06403 (.00005)	1.00508 (.00004)	0.95428 (.00004)
Diff	1726.00 pcm (7.1 pcm)	2218.00 pcm (6.7 pcm)	2699.00 pcm (6.7 pcm)

Clearly, linear anisotropy with no energy-angle coupling within energy groups is not sufficient to closely match continuous energy results. Increasing the number of cross section energy groups would improve the results; however, the linear anisotropy is likely to be the stronger effect since this is a fast reactor. Additionally, increasing the number of cross section groups complicates methods development. As a result, larger errors can be tolerated to make methods development easier. With all of this in mind, a brief fission density comparison between the two near critical cases will be presented.

As previously discussed, the eigenvalue results for this comparison were significantly off. The fission density results suffered similarly. Relative errors between the two models will be presented below in Table 12, along with other relevant quantities such as the average absolute relative error, the root mean square (RMS) error, the mean relative error (MRE), and the maximum absolute error. The relative error of a given quantity is defined below in Equation 1, where V is some value and V_{ref} is that same value in the reference model. The additional quantities listed are also defined in Equations 2 and 3 where fd_p is the fission density of a given fuel pin p, #p is the total number of fuel pins, and the summation is over all pins in the core. In this comparison, the continuous energy model will be the reference point.

$$RE = \frac{V - V_{ref}}{V_{ref}} \tag{1}$$

$$AVG = \frac{\sum_p |RE_p|}{\#p} \times 100\% \quad (2)$$

$$MRE = \frac{\sum_p |RE_p| * fd_p}{\#p} \times 100\% \quad (3)$$

Table 12.Continuous Energy to 15 Group Comparison Quantities – Near Critical

Difference in k-eff (pcm)	2218
$\sigma_{k\text{-}eff}$ CE (pcm)	5
$\sigma_{k\text{-}eff}$ 15g (pcm)	4
Pin AVG Absolute RD (%)	11.693
Pin RMS (%)	13.950
Pin MRE (%)	11.369
Pin Max Absolute RD (%)	30.599
Max σ_{pin} CE (%)	0.7000
Avg σ_{pin} CE (%)	0.2276
Min σ_{pin} CE (%)	0.1200
Max σ_{pin} 15g (%)	0.2500
Avg σ_{pin} 15g (%)	0.1381
Min σ_{pin} 15g (%)	0.1100

The pin fission density distribution for the continuous energy case is presented in Figure 10. The fission densities were normalized such that the average pin in the core has a value of 1 for its fission density.

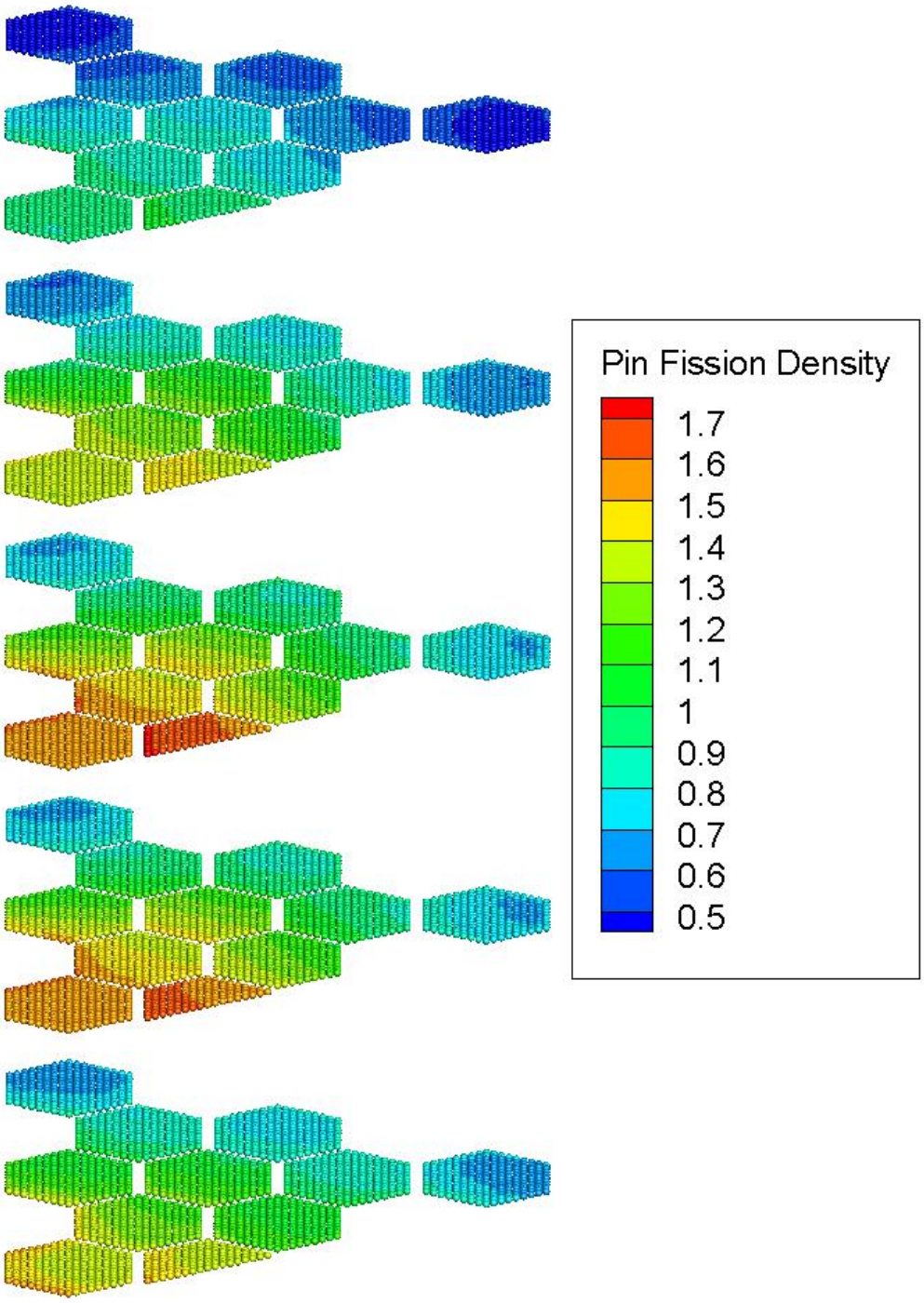

Figure 9. Continuous Energy Near Critical Pin Fission Densities

Following in Figure 11 is a plot of the uncertainties associated with the continuous energy pin fission densities. As expected, the uncertainty peaks at the edges of the model where the statistics are inevitably worse.

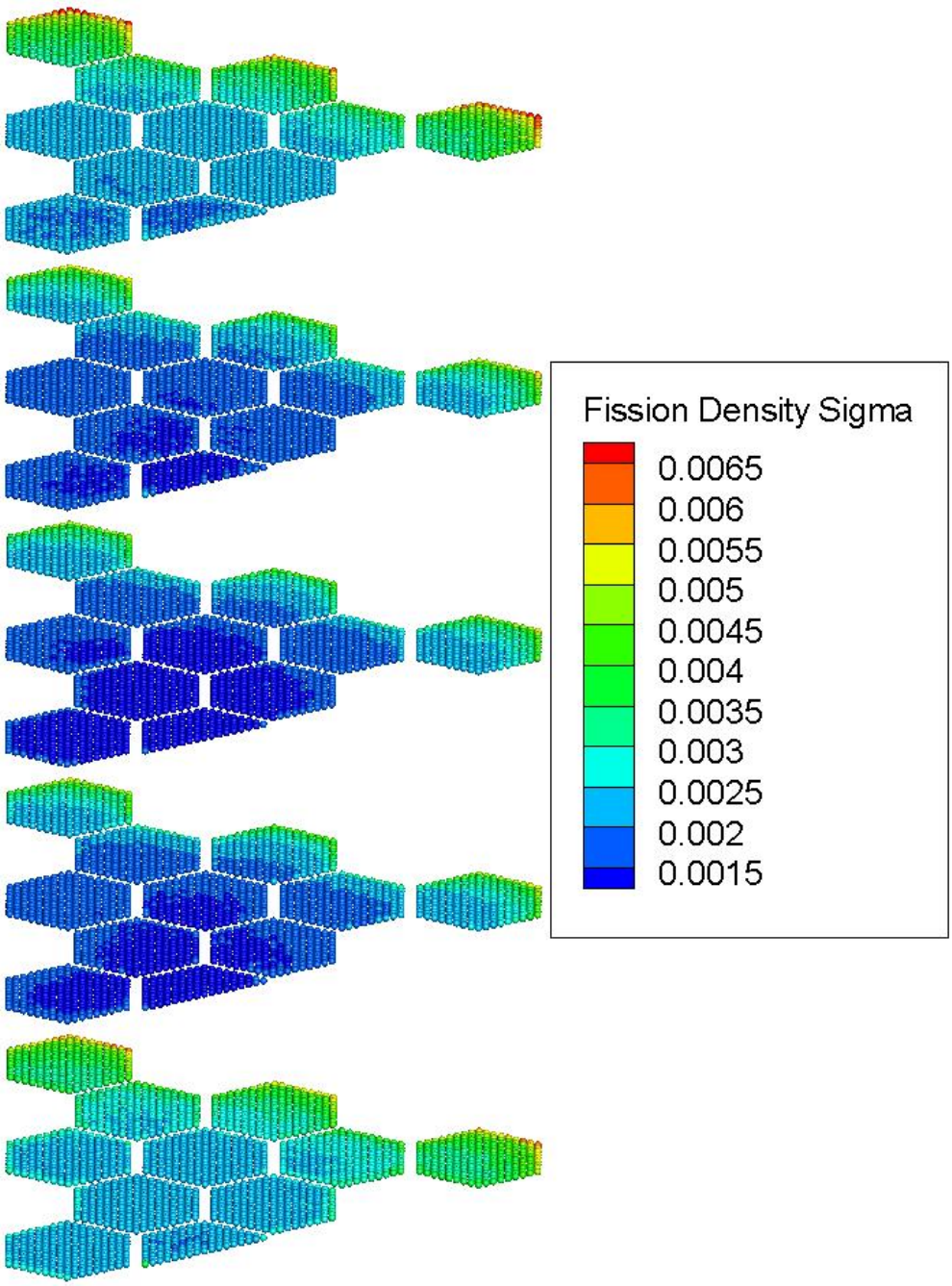

Figure 10. Continuous Energy Near Critical Pin Fission Density Uncertainties

Clearly the 15 group cross section library yields eigenvalues and fission densities with a significant difference relative to the continuous energy. Investigations into improving cross section generation would be beneficial, but are outside the scope of this paper. Again, the purpose of this benchmark is not to investigate cross sections, but method verification. As a result, some error in cross sections can be tolerated with the understanding that both codes will be supplied identical cross sections.

CHAPTER 6

COMET SOLUTION

COMET is a Coarse-Mesh Transport Method that has been proven in heterogeneous 3-D hexagonal geometry[6]. As previously stated, the goal of this paper is to further prove COMET for a similar geometry in a fast reactor environment.

An in depth explanation of COMET is too involved to be included here (but can be found from Mosher and Rahnema 2006 (TTSP)[9], Connolly et al. 2011[7], Zhang and Rahnema 2012 (ANE)[10], and from Connolly and Rahnema 2013[6]) However, a brief overview of the process will be given. Of the references cited above, the two involving Connolly have a focus on hexagonal geometry while the other two are focused on general COMET methodology.

This is an incident flux response function expansion method that solves the transport equation throughout the entire core. First, the core is divided into a grid of coarse meshes of assembly size, and then the angular flux is expanded at the mesh boundaries using discrete Legendre polynomials. Next, depending on the version of COMET in use, the response functions for the coarse meshes are generated using transport discrete ordinates or stochastic methods. In this particular case, stochastic Monte-Carlo methods were used for response function generation. Finally, the whole-core calculation is performed using a deterministic iterative method with an inner and outer loop. The outer iterations act on the global eigenvalue, while the inner iterations are on the partial currents crossing coarse meshes. COMET is an advancement on older response matrix methods because it relies purely on transport theory and because of its ability to model exact core, lattice, and fuel pin heterogeneous specifications without the need for homogenization. Additionally, COMET is also advantageous for its arbitrarily

high accuracy of mesh boundary conditions and its ability to model many different reactor types and geometries. The COMET method is given further consideration below in order to establish appropriate background knowledge, for more information on traditional high-order response matrix theory, see Stamm'ler and Abbate (1983).

Equation 4a represents the steady state neutron transport equation over an arbitrary volume with a general boundary condition presented in equation 4b:

$$\begin{aligned}\hat{\Omega}\cdot\nabla\phi(\vec{r},\hat{\Omega},E)+\ \sigma_t(\vec{r},E)\phi(\vec{r},\hat{\Omega},E)\\ =\ \int_0^\infty dE'\ \int_{4\pi} d\hat{\Omega}'\,\sigma_s(\vec{r},\hat{\Omega}',E'\rightarrow\ \hat{\Omega},E)\phi(\vec{r},\hat{\Omega}',E')\\ +\ \frac{1}{4\pi}\,\chi(\vec{r},E)\ \int_0^\infty dE'\ \int_{4\pi} d\hat{\Omega}'\ \times\ \frac{\upsilon\sigma_f(\vec{r},E')}{k}\,\phi(\vec{r},\hat{\Omega}',E')\end{aligned}\qquad (4a)$$

$$\phi(\vec{r}_b,\hat{\Omega},E)=B(\vec{r}_b,\hat{\Omega}',E'),\qquad \hat{n}\cdot\hat{\Omega}<0\quad and\quad \hat{n}\cdot\hat{\Omega}'>0 \qquad (4b)$$

Where ϕ represents the angular flux of neutrons defined for each point $\vec{r}$, travelling in direction $\hat{\Omega}$, with energy E within the volume. Macroscopic cross sections for total, scattering, and fission are represented as σ_t, σ_s, and σ_f respectively. The fission energy spectrum is represented as χ with an average of υ neutrons per reaction. The core multiplication factor is represented by k. In equation 4b, $\vec{r}_b$ represents a point at the boundary of the volume with an outward normal $\hat{n}$.

The first step in the COMET process consists of dividing the overall volume into a set of smaller volumes referred to as coarse meshes. The transport equation for each of these coarse meshes can be written as:

$$\hat{\Omega} \cdot \nabla\psi(\vec{r}, \hat{\Omega}, E) + \sigma_t(\vec{r}, E)\psi(\vec{r}, \hat{\Omega}, E)$$
$$= \int_0^\infty dE' \int_{4\pi} d\hat{\Omega}' \, \sigma_s(\vec{r}, \hat{\Omega}', E' \rightarrow \hat{\Omega}, E)\psi(\vec{r}, \hat{\Omega}', E') + \frac{1}{4\pi} \chi(\vec{r}, E) \int_0^\infty dE' \int_{4\pi} d\hat{\Omega}'$$
$$\times \frac{\upsilon\sigma_f(\vec{r}, E')}{k} \psi(\vec{r}, \hat{\Omega}', E')$$
$$+ Q_i(\vec{r}, \hat{\Omega}, E) \quad (5)$$

Where ψ represents the solution to the coarse mesh transport equation within mesh i. In equation 5, the core multiplication factor k is fixed, since it represents a property of the full core geometry rather than the coarse mesh itself. It exists to scale the fission term, which allows for coarse meshes to be solved at different values of k. Q_i can be used to denote an external source, however in this case there is no external source. An incoming boundary condition on the mesh surface is used instead. This allows each individual mesh to be coupled to adjacent meshes by a particle balance at the mesh interface. Angular flux has been shown to be an accurate boundary condition using this method.

COMET determines the outgoing condition of the mesh boundary as a response to give a certain incoming boundary condition. This process continues for each face of each unique mesh within the core for each expansion order. Where this sum truncates is chosen by the user in order to balance the accuracy of the solution with the computational requirements of running the model.

Coarse mesh calculations are performed using several different values of k (0.9, 1.0, and 1.1 here). This allows for the determination of a desired response function simply by interpolating the existing values using the systems multiplication factor.

The full core problem is solved iteratively using initial guesses for the multiplication factor and either the flux or current distribution. A deterministic sweep is used to calculate new response functions using the pre-compiled library from coarse mesh calculations and the linear superposition of those previous solutions. From there,

the mesh interface conditions are updated and the process continues until the desired level of convergence is met. At this point, the core eigenvalue is computed using neutron balance and the whole process repeats until a desired level of convergence is reached on the multiplication factor.

The first step for using COMET is to create single assembly models for each unique assembly present in the core. Those models are then used to generate comet response functions for each structure which are then compiled into a database. Finally, the user specifies a full core design constructed from the component parts modeled in the first step. This design allows for reconfigurations of the core to be run without generating new response functions. Once response functions are generated, COMET is immensely faster than MCNP. For this particular benchmark, the COMET model is almost three orders of magnitude faster. As a result of the fact that core geometries do not change but fuel loading patterns are frequently investigated, COMET has significant advantages.

Comet Model

To verify the accuracy of COMET, it is tested against whole core Monte Carlo benchmarks using MCNP as the numerical benchmark. As previously discussed, the three cases considered are ARO, NC, and ARI. The geometry of each case is identical to the geometry used previously. A single response expansion coefficient library was created for this problem using 0.90, 1.00, and 1.10 as the discrete values for the core multiplication factor to model. 100 million incoming surface source particles were simulated per unique coarse mesh face and expansion order. For a second order spatial expansion with fourth order angular expansion, the library was 14.06 GB of disk space and required 296 cpu days total, distributed between 48 CPUs, to generate. Hard drive space has thus far been the limiting factor in the completion of higher order expansions, however this expansion order has produced strong results implying higher orders may be

unnecessary. The completed library represents a small fraction of the response function data in terms of hard drive space and higher order expansions require large amounts of space, on the order of hundreds of gigabytes, to run. The size of the response expansion coefficient library is proportional to the square of the number of expansion orders used. The MCNP runs used the same number of particles in the same number of cycles as previously defined. Additionally, runs were performed using second order spatial and angular expansions to gauge how sensitive the results were to angular expansion order. Both sets of results are presented in the following sections, however only the higher spatial expansion results are plotted.

Results Comparison

The core eigenvalue comparison between MCNP and COMET can be found below in Table 13. It contains the eigenvalues for the MCNP runs, the COMET runs and the difference between the COMET and the MCNP values.

Table 13. Eigenvalues Comparison and (Standard Deviation)

	ARO	NC	ARI
MCNP	1.06403 (.00005)	1.00508 (.00004)	0.95428 (.00004)
COMET 2244	1.06359 (.00048)	1.00451 (.00043)	0.95402 (.00039)
Diff	44 pcm (48.3 pcm)	57 pcm (43.2 pcm)	26 pcm (39.2 pcm)
COMET 2222	1.06375 (.00048)	1.00476 (.00043)	0.95423 (.00039)
Diff	28 pcm (48.3 pcm)	32 pcm (43.2 pcm)	5 pcm (39.2 pcm)

As with the continuous energy comparison, a series of relevant quantities will be presented followed by a mapping of the pin fission densities, their uncertainties for each model, and finally a mapping of the relative difference between the MCNP and COMET models. For each case, the MCNP model was considered the reference model.

The eigenvalue results for this comparison showed good agreement. The ARO and ARI cases are within one COMET standard deviation with the NC model roughly one and a third standard deviations off. The lower expansion order results are actually closer to the MCNP eigenvalue results; however, the differences are small relative to the uncertainties in the COMET results. The fission density results are very accurate; with the ARO case having the highest average relative difference of less than half a percent. In this case, the higher angular expansion order model produced better results by a small margin. Looking at both eigenvalue and pin fission density results implies that the higher angular expansion order is unnecessary for accurate results in this particular core configuration.

Relevant quantities such as the average absolute relative difference, the root mean square (RMS) error, the mean relative error (MRE), and the maximum absolute error are presented below in Table 14.

Table 14.MCNP to COMET Comparison

	ARO		NC		ARI	
Model Expansion Orders	2244	2222	2244	2222	2244	2222
Difference in k-eff (pcm)	44	28	57	32	26	5
$\sigma_{k\text{-}eff}$ MCNP (pcm)	5		4		4	
$\sigma_{k\text{-}eff}$ COMET (pcm)	48	48	43	43	39	39
Pin AVG Absolute RE (%)	0.4126	0.4147	0.4055	0.4144	0.4039	0.4161
Pin RMS (%)	0.5334	0.5257	0.5218	0.5289	0.5156	0.5343
Pin MRE (%)	0.4139	0.4217	0.4105	0.4224	0.4077	0.4205
Pin Max Absolute RE (%)	1.8582	1.7992	1.6737	1.6737	1.7691	2.0291
Max σ_{pin} MCNP (%)	0.2300		0.2500		0.2500	
Avg σ_{pin} MCNP (%)	0.1430		0.1381		0.1464	
Min σ_{pin} MCNP (%)	0.1000		0.1100		0.1100	
Max σ_{pin} COMET (%)	0.0200	0.0200	0.0200	0.0200	0.0200	0.0200
Avg σ_{pin} COMET (%)	0.0128	0.0125	0.0125	0.0128	0.0131	0.0130
Min σ_{pin} COMET (%)	0.0100	0.0100	0.0100	0.0100	0.0100	0.0100

From the results it can be seen that COMET has strong agreement in pin fission densities. Following in Figures 12 through 17 are plots of pin fission densities and the associated uncertainty for each of the six models. After that, Figures 18 through 20 will show maps of the relative error between the two models. The relative error plots include a full plot with the legend on the left hand side. Then in the middle is the plot only including values less than zero. Finally on the right hand side is a plot with only values greater than zero. This separation was done to make the plots easier to interpret. As a result of using the MCNP model as the reference model, locations where the relative error is negative indicate that COMET overestimated relative to MCNP, with the reverse being true for locations where the relative error is positive.

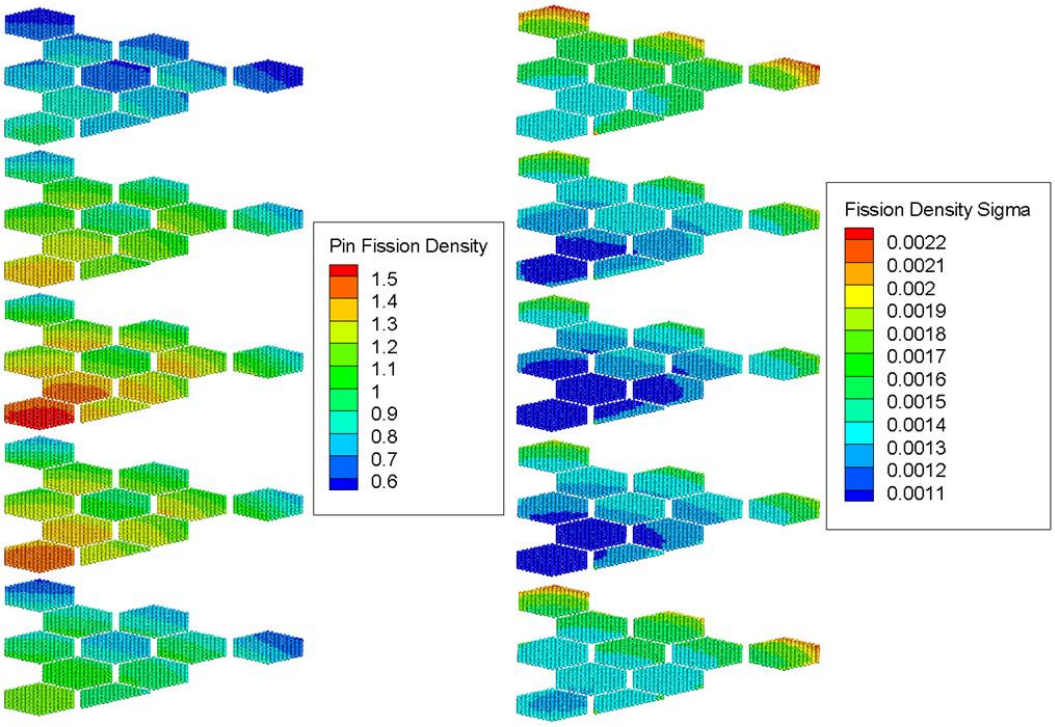

Figure 11. MCNP ARO Fission Densities and Uncertainties

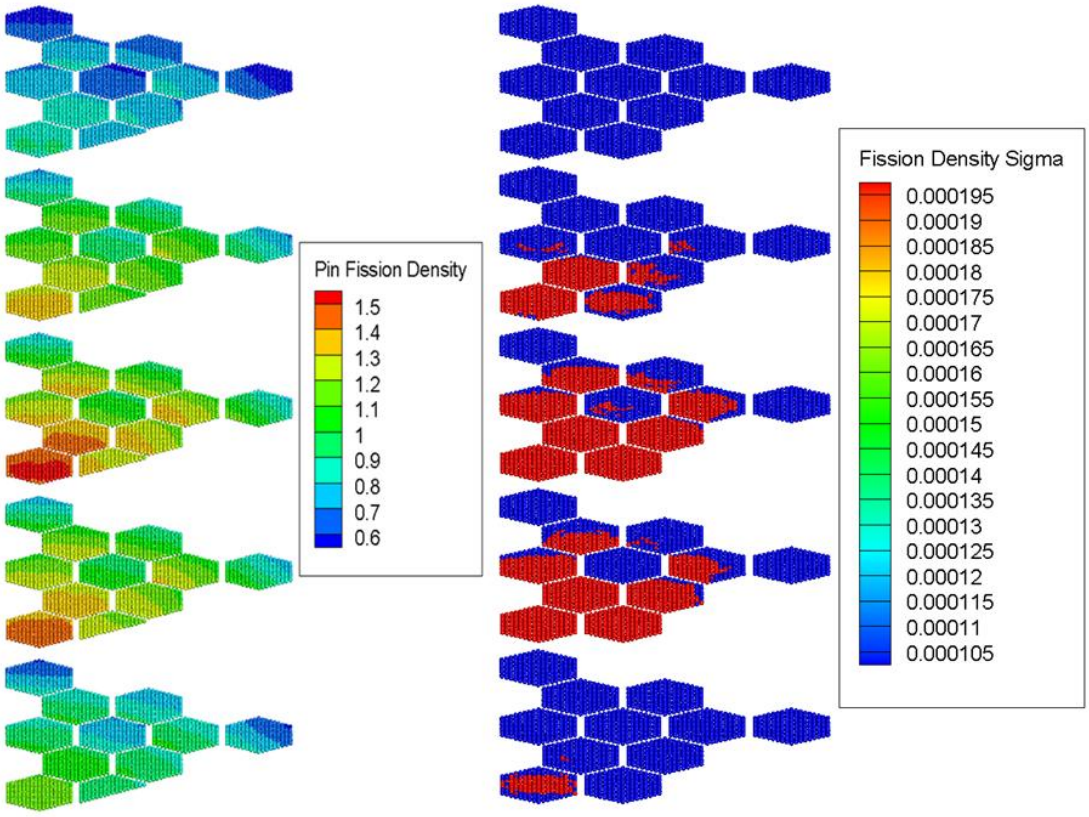

Figure 12. COMET ARO Fission Densities and Uncertainties

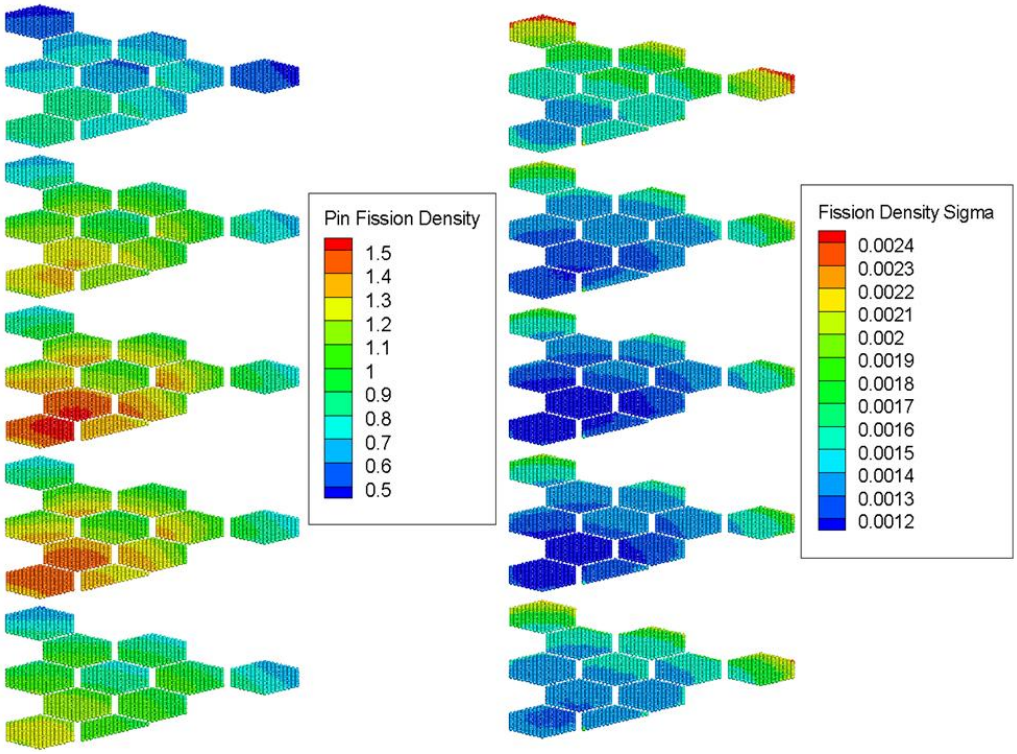

Figure 13. MCNP NC Fission Densities and Uncertainties

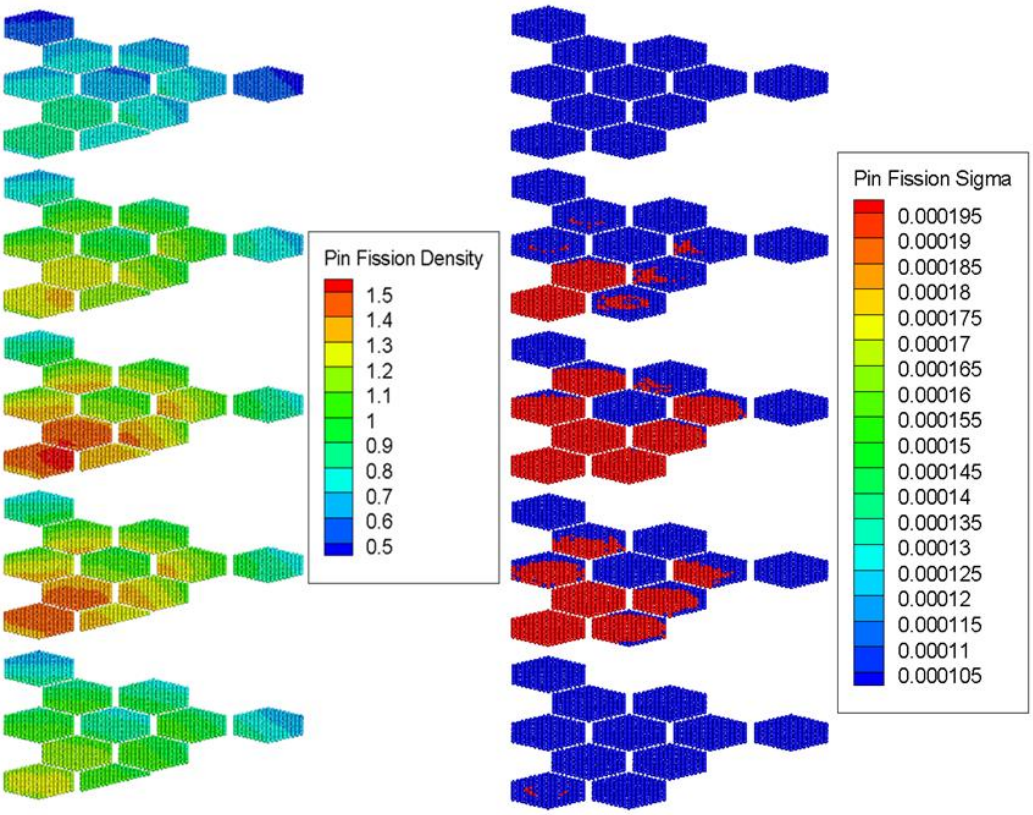

Figure 14. COMET NC Fission Densities and Uncertainties

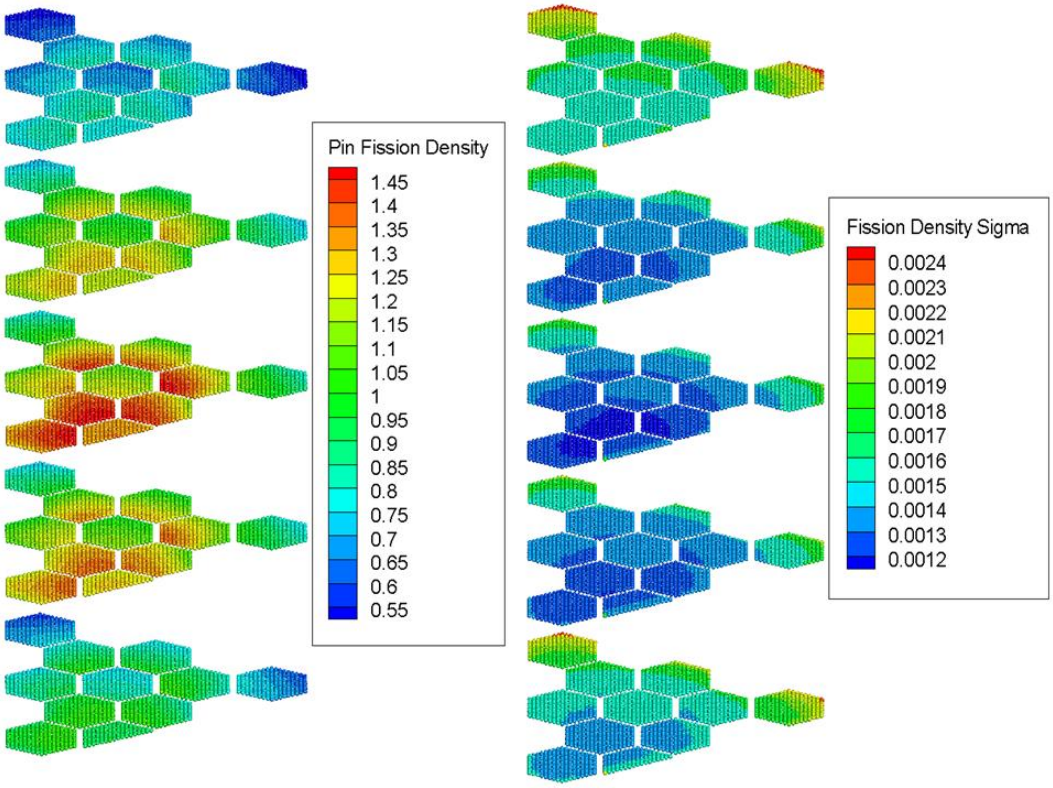

Figure 15. MCNP ARI Fission Densities and Uncertainties

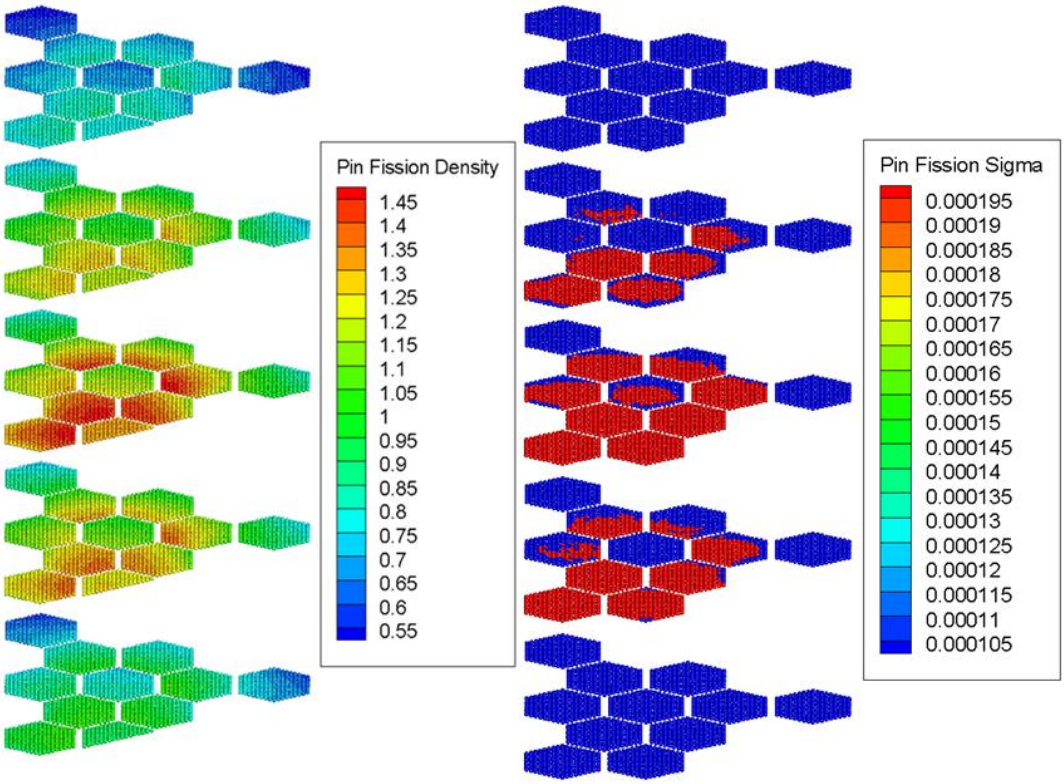

Figure 16. COMET ARI Fission Densities and Uncertainties

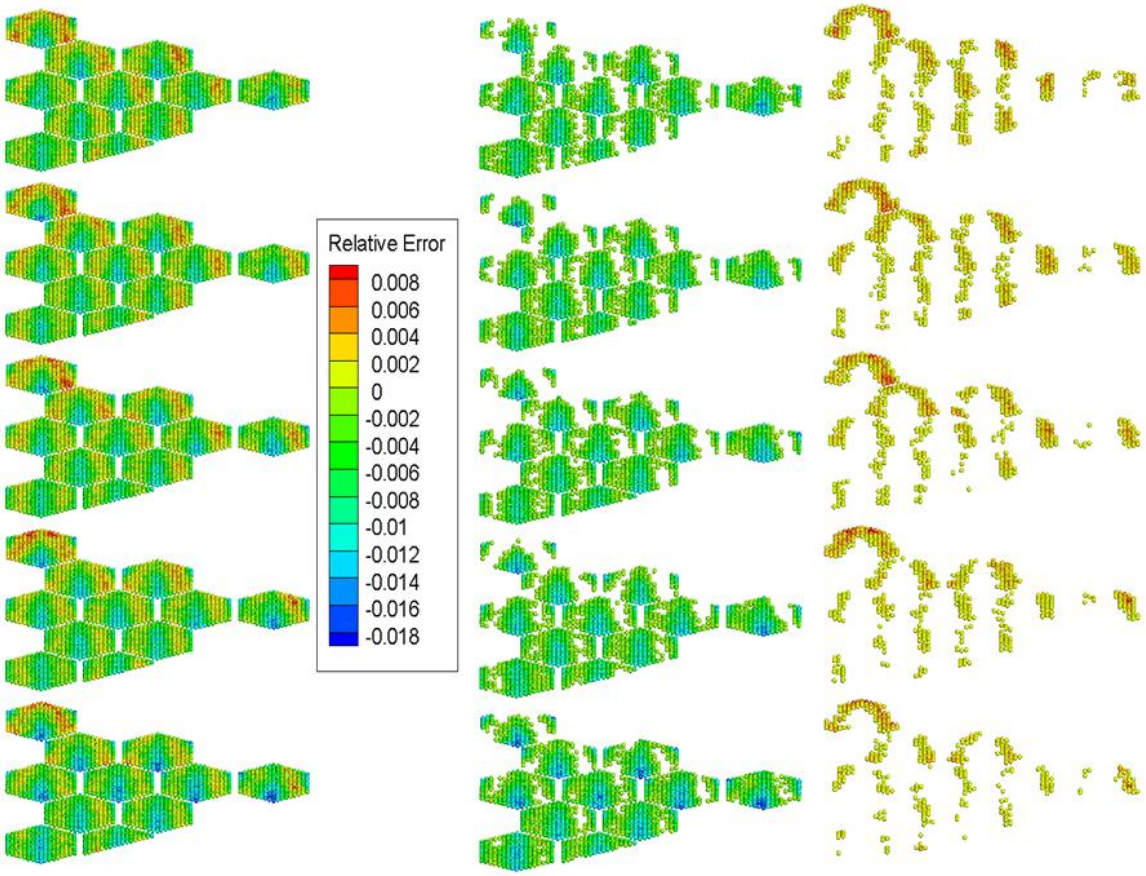

Figure 17. ARO Relative Error Map

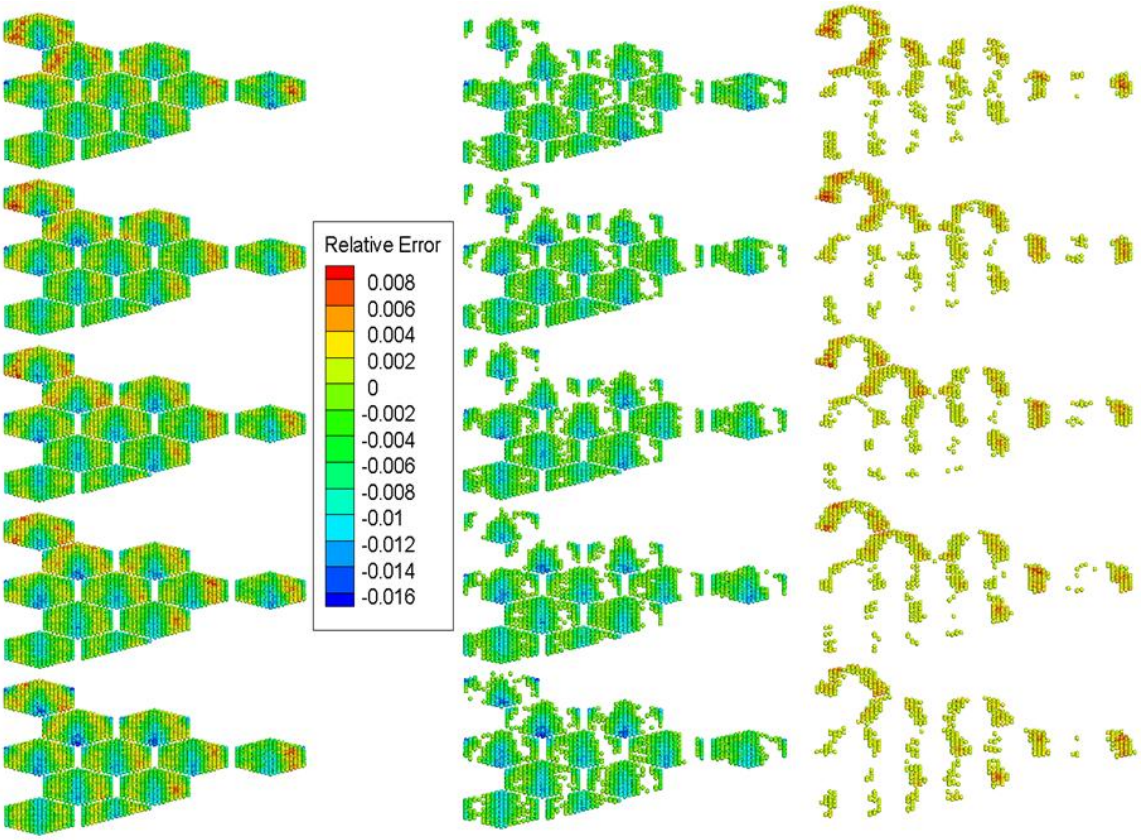

Figure 18. NC Relative Error Map

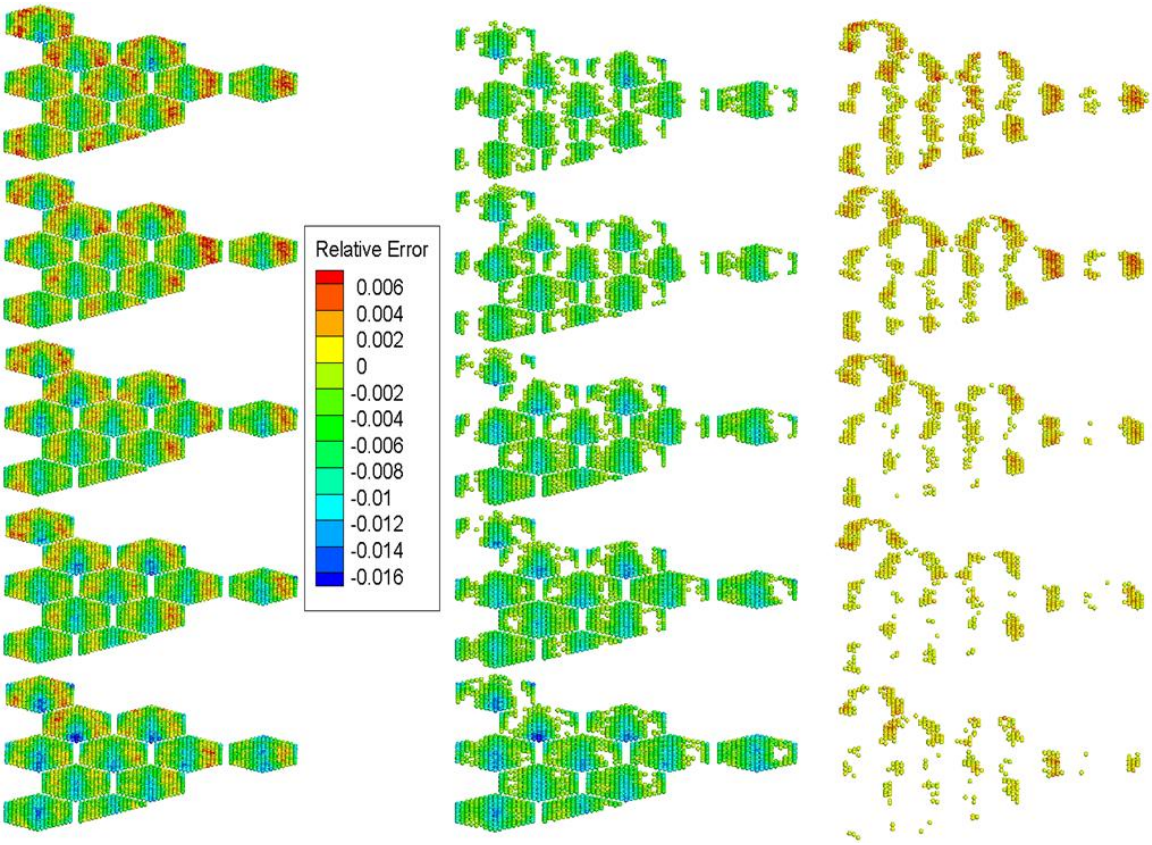

Figure 19. ARI Relative Error Map

The uncertainties on the COMET model pin fission densities are so small that the truncation leads to only two values (0.000100 – 0.000200, with an average of 0.000128). This results in the strange plots that only have extremes. In reality the difference between the higher uncertainties and lower uncertainties is extremely small.

The only patterns that are apparent from the relative error plots is that the largest differences between the models tends to occur near the edge of each assembly, where the expansion order approximation is taking place, and in the sections of the core experiencing less flux, such as the bottom level.

Finally, in Appendix C are the assembly average pin fission density distributions for MCNP divided into assembly meshes. Also in Appendix C are the MCNP coordinates and pin fission densities for two assembly meshes: the peak assembly mesh of the near critical configuration (Assembly 1, Mesh 3) and a high leakage assembly

mesh of the near critical configuration (Assembly 9, Mesh 5). These quantities are included because they are useful for benchmarking comparisons in this particular core where there are far too many fuel pins to compare directly (11935 fuel pins for merely one-sixth of the core.

Peaking Factors

For the sake of including other quantities of interest, included below in Tables 15 and 16 are the MCNP measured peaking factors of each fuel assembly in the core and the difference between MCNP and COMET in percent for the same quantity. The core peaking factors are a ratio of the maximum pin fission density in a given assembly to the overall core average, which was normalized to one. It does take into consideration the 5 axial levels. In order to accomplish this, a numbering scheme for the relevant assemblies is necessary. Below in Figure 20 is the numbering scheme for the core. Both models show good agreement, with an average difference of -0.6152% and a greatest difference of -1.9083%.

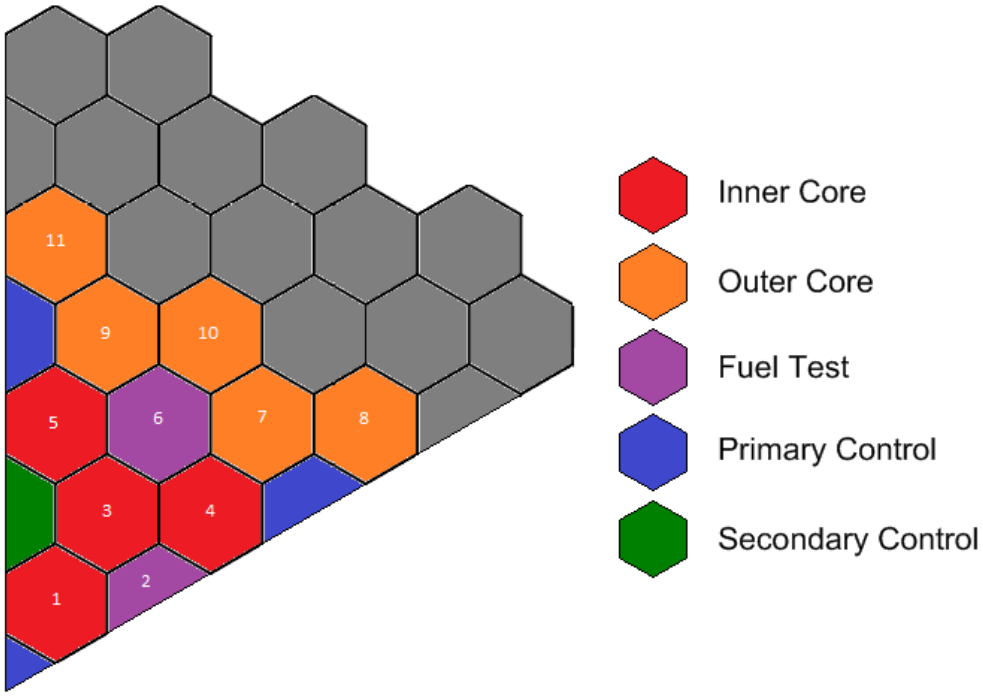

Figure 20. One-Sixth Symmetry Core with Assembly Numbering

Table 15. Core Peaking Factors

Peaking Factor			
Assembly	ARO	NC	ARI
1	1.533	1.5213	1.4665
2	1.5035	1.4504	1.4712
3	1.3721	1.3289	1.3055
4	1.4284	1.3709	1.4506
5	1.3704	1.327	1.3488
6	1.2027	1.1518	1.2176
7	1.4031	1.3908	1.4894
8	0.9979	1.1415	1.096
9	1.3717	1.3643	1.415
10	1.2898	1.2574	1.3795
11	0.9891	1.1168	1.054

Table 16. MCNP - COMET Peaking Factor Different (%)

Peaking Factor			
Assembly	ARO	NC	ARI
1	-0.0247	-0.5622	-0.1510
2	-1.3727	-0.5302	-0.2647
3	-1.4707	-1.5308	-0.3723
4	-0.3704	-0.2507	-0.2239
5	-0.4362	-0.4392	-0.6017
6	-0.4133	-0.2951	-1.1558
7	-0.4341	-0.4080	-0.5157
8	-0.6201	-0.1193	-0.7437
9	-1.6827	-1.9083	-1.4565
10	0.0805	0.0606	-0.5848
11	0.0402	-1.4825	-0.0628

Control Rod Worth

Finally, included in Table 17 is a presentation of control rod assembly worth values. It is worth reiterating that the control rods move in entire assemblies in this core configuration, not in single rods. Four different control rod locations were tested based on the one-sixth core geometry: the central control rod assembly, the secondary control

rod assembly, and the two edge control rod assemblies. The numbering scheme identifying these control rods is presented below in Figure 21. The models compare favorably, with only one control rod worth difference falling outside a single standard deviation. Even then, it is well within one and a third standard deviations. These worth value were gathered simply by comparing the eigenvalue of the ARO version, to models where the target rod is fully inserted.

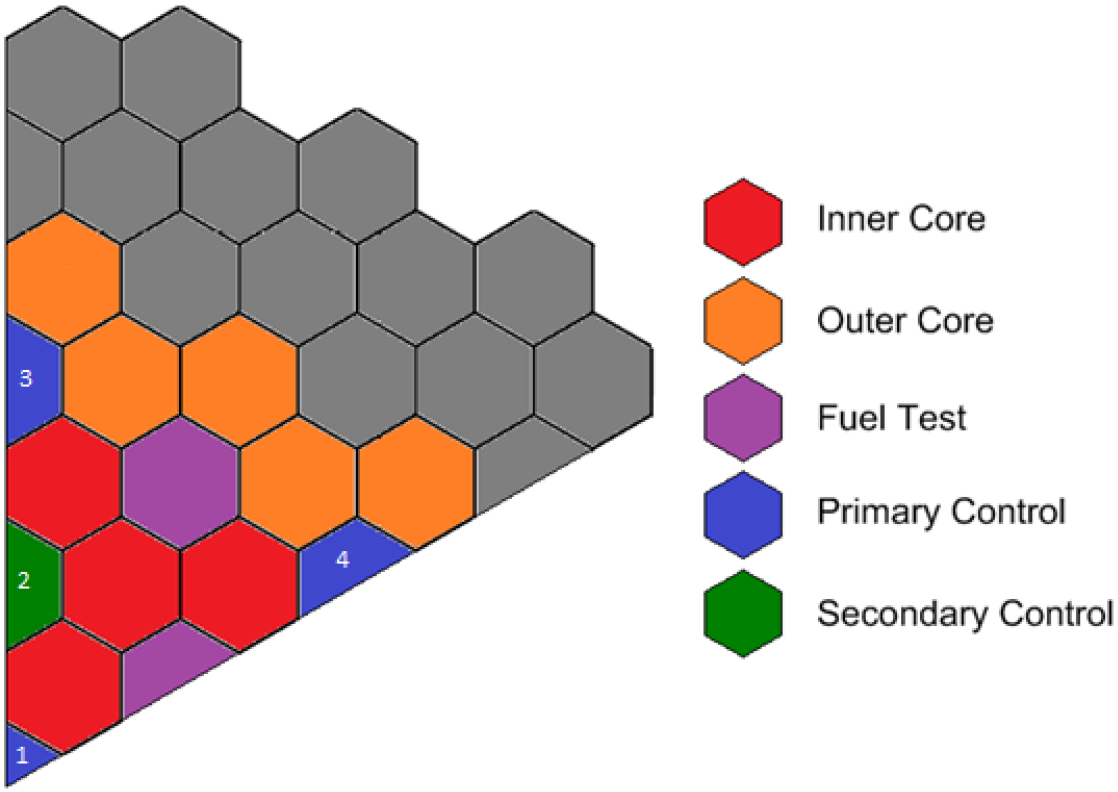

Figure 21. Control Rod Assembly Numbering

Table 17. Control Rod Worth and (Uncertainty)

Control Rod Location	MCNP Computed Worth (pcm)	COMET Computed Worth (pcm)	Difference (pcm)
1	1874 (7.1)	1876 (63.7)	-2 (64.1)
2	821 (7.8)	746 (64.4)	-75 (64.9)
3	789 (22.6)	762 (64.4)	27 (68.3)
4	1572 (7.8)	1524 (63.7)	48 (64.2)

The location tested using both codes shows extremely strong agreement between MCNP and COMET.

Runtime Comparison

A significant advantage to COMET is its fast runtime relative to MCNP so it would be remiss not to touch on the subject of model runtime. All computer time values assume a scaling factor of unity as you increase the number of processors employed. Additional differences that should be noted: MCNP converges the eigenvalue much faster than COMET because it uses three different methods of computing it to COMET's single method, however COMET gets much smaller uncertainty on fission densities because of its method of solving within coarse meshes. All of this is reflected below in Table 18. It is important to realize that for all of these models, COMET was solved on the full core model without any symmetry applied while MCNP was using one sixth symmetry.

Table 18. Runtime and Uncertainty Comparison

	Runtime (cpu hrs)	Eigenvalue Uncertainty (pcm)	Fission Density Uncertainty Range (%)
COMET ARO	14.62	48	0.01 - 0.02
MCNP ARO	9289	5	0.10 - 0.23
COMET NC	20.12	43	0.01 - 0.02
MCNP NC	8965	4	0.11 - 0.25
COMET ARI	22.98	39	0.01 - 0.02
MCNP ARI	8785	4	0.11 - 0.25

CHAPTER 7

CONCLUSION

In this paper, we have developed three configurations of a stylized 3-dimensional advanced burner test reactor benchmark problem. Although stylized, it was based on the ANL ABTR design and care was taken to maintain the physics of the fast spectrum system despite the high degree of simplification that was applied. The material specification is the same as the original design and is included in the appendices of this paper.

A 15 group cross section library was developed for the direct comparison of different transport codes using this benchmark based on a literature search of viable fast system group structures. The linear anisotropy and lack of in group angle-energy coupling lead to significant differences between the continuous energy and 15 group calculations. This was considered acceptable as the goal herein is methods verification rather than cross section verification and a set of common cross sections is extremely important for evaluating different methods.

Next, COMET was benchmarked against MCNP with strong results using second order spatial and fourth order angular Legendre expansions. Lower order COMET models were also performed using second order spatial and angular Legendre expansions with only relatively small decreases in the accuracy of results.

Finally, peaking factors were computed and a runtime comparison between MCNP and COMET was made. The MCNP computed peaking factors compared favorably with the COMET versions and the runtime comparison highlights the computational advantage COMET has when compared to MCNP.

APPENDIX A

MATERIALS SPECIFICATIONS

All data contained in this appendix is directly from ANL. It is included here for the sake of completeness so that the reader may generate their own cross sections if necessary.

1. Lower Structure

Na	1.5591E-02
Fe	1.5878E-02
Ni	3.2604E-03
Cr	3.2355E-03
Mn55	5.0846E-04
Mo	4.3524E-04

2. Lower Reflector of fuel assembly

	Heterogeneous			Homogeneous
	Clad & str.	Coolant	Duct	
Na		2.2272E-02		7.1455E-03
Fe	6.9844E-02		6.9844E-02	4.7436E-02
Ni	4.3063E-04		4.3063E-04	2.9248E-04
Cr	1.0385E-02		1.0385E-02	7.0532E-03
Mn55	4.6007E-04		4.6007E-04	3.1247E-04
Mo	4.9097E-04		4.9097E-04	3.3346E-04

3. Active Fuel

Nuclide	Heterogeneous			Clad	Coolant	Duct
	inner core	middle core	out core	HT9	Sodium	HT9
U-234	1.2225E-08	1.0027E-06	1.4997E-08			
U-235	3.2248E-05	3.2038E-05	3.1767E-05			
U-236	2.0561E-06	1.9484E-06	1.8593E-06			
U-238	2.0222E-02	1.9745E-02	1.9317E-02			
Np237	3.8387E-06	1.8093E-04	3.1274E-06			
Pu236	1.3918E-11	9.0759E-10	9.1074E-12			
Pu238	9.5854E-07	9.0509E-05	9.8743E-07			
Pu239	3.4991E-03	2.3546E-03	4.3068E-03			
Pu240	3.7398E-04	1.0881E-03	4.5617E-04			
Pu241	2.4535E-05	2.9432E-04	2.9545E-05			
Pu242	1.7542E-06	2.1919E-04	2.0615E-06			
Am241	1.4209E-06	2.1306E-04	2.2274E-06			
Am242m	2.8475E-08	5.8336E-06	4.0761E-08			
Am243	6.1338E-08	4.3624E-05	7.5588E-08			
Cm242	4.7083E-08	7.3545E-06	5.6294E-08			
Cm243	7.4138E-10	2.4428E-07	9.0540E-10			
Cm244	4.8305E-09	1.0986E-05	5.5302E-09			
Cm245	1.9064E-10	9.7716E-07	1.9972E-10			
Cm246	2.6112E-12	6.7680E-08	2.4070E-12			
Zr	7.2938E-03	7.2938E-03	7.2938E-03			
Na					2.2272E-02	
Fe				6.9844E-02		6.9844E-02
Ni				4.3063E-04		4.3063E-04
Cr				1.0385E-02		1.0385E-02
Mn55				4.6007E-04		4.6007E-04
Mo	9.76123E-04	8.36399E-04	9.81845E-04	4.9097E-04		4.9097E-04

Nuclide	Homogeneous		
	Inner core	Test fuel	Outer core
U-234	5.46898E-09	4.48578E-07	6.70877E-09
U-235	1.44262E-05	1.43324E-05	1.42111E-05
U-236	9.19798E-07	8.71638E-07	8.31760E-07
U-238	9.04638E-03	8.83280E-03	8.64147E-03
Np237	1.71727E-06	8.09410E-05	1.39907E-06
Pu236	6.22636E-12	4.06014E-10	4.07421E-12
Pu238	4.28807E-07	4.04893E-05	4.41730E-07
Pu239	1.56532E-03	1.05336E-03	1.92666E-03
Pu240	1.67301E-04	4.86743E-04	2.04069E-04
Pu241	1.09760E-05	1.31667E-04	1.32172E-05
Pu242	7.84751E-07	9.80540E-05	9.22204E-07
Am241	6.35636E-07	9.53142E-05	9.96453E-07
Am242m	1.27384E-08	2.60969E-06	1.82346E-08
Am243	2.74399E-08	1.95154E-05	3.38145E-08
Cm242	2.10628E-08	3.29008E-06	2.51831E-08
Cm243	3.31661E-10	1.09281E-07	4.05034E-10
Cm244	2.16096E-09	4.91452E-06	2.47394E-09
Cm245	8.52838E-11	4.37138E-07	8.93442E-11
Cm246	1.16811E-12	3.02767E-08	1.07680E-12
Zr	3.26289E-03	3.26289E-03	3.26289E-03
Na	7.14528E-03	7.14528E-03	7.14528E-03
Fe	1.61921E-02	1.61921E-02	1.61921E-02
Ni	9.98349E-05	9.98349E-05	9.98349E-05
Cr	2.40756E-03	2.40756E-03	2.40756E-03
Mn55	1.06659E-04	1.06659E-04	1.06659E-04
Mo	5.50492E-04	4.87986E-04	5.53051E-04

- Na density of homogeneous voided case is 1.2039E-3

4. Gas plenum of fuel assembly with displaced sodium bond

	Heterogeneous			Homogeneous
	Clad	Coolant	Duct	
Na		2.2272E-02		1.7109E-02
Fe	6.9844E-02		6.9844E-02	1.6192E-02
Ni	4.3063E-04		4.3063E-04	9.9831E-05
Cr	1.0385E-02		1.0385E-02	2.4075E-03
Mn55	4.6007E-04		4.6007E-04	1.0666E-04
Mo	4.9097E-04		4.9097E-04	1.1382E-04

- Na density of homogeneous voided case is 1.1167E-2

5. Gas plenum of fuel assembly without displaced sodium bond

	Heterogeneous			Homogeneous
	Clad	Coolant	Duct	
Na		2.2272E-02		7.1455E-03
Fe	6.9844E-02		6.9844E-02	1.6192E-02
Ni	4.3063E-04		4.3063E-04	9.9831E-05
Cr	1.0385E-02		1.0385E-02	2.4075E-03
Mn55	4.6007E-04		4.6007E-04	1.0666E-04
Mo	4.9097E-04		4.9097E-04	1.1382E-04

- Na density of homogeneous voided case is 1.2039E-3

6. Empty under Control Rod

	Heterogeneous		Homogeneous
Nuclide	Coolant	Duct	
Na	2.2272E-02		2.0529E-02
Fe		6.9844E-02	5.4661E-03
Ni		4.3063E-04	3.3702E-05
Cr		1.0385E-02	8.1273E-04
Mn55		4.6007E-04	3.6006E-05
Mo		4.9097E-04	3.8424E-05

7. Control rod follower

	Heterogeneous			Homogeneous
Nuclide	Follower	Coolant	Duct	
Na		2.22724E-02		1.1051E-02
Fe	5.2048E-02		6.9844E-02	2.7616E-02
Ni	1.0687E-02		4.3063E-04	4.5819E-03
Cr	1.0606E-02		1.0385E-02	5.3263E-03
Mn55	1.6667E-03		4.6007E-04	7.4530E-04
Mo	1.4267E-03		4.9097E-04	6.4558E-04

8. Control rod

	Heterogeneous				Homogeneous
Nuclide	Absorber	Clad	Coolant	Duct	
C	4.0679E-03				1.4834E-03
B10	1.6441E-02				5.9956E-03
B11	6.6179E-02				2.4133E-02
Na			2.2272E-02		8.1722E-03
Fe		6.9844E-02		6.9844E-02	1.8747E-02
Ni		4.3063E-04		4.3063E-04	1.1559E-04
Cr		1.0385E-02		1.0385E-02	2.7875E-03
Mn55		4.6007E-04		4.6007E-04	1.2349E-04
Mo		4.9097E-04		4.9097E-04	1.3179E-04

9. Gas plenum of control rod

	Heterogeneous			Homogeneous
Nuclide	Clad	Coolant	Duct	
Na		2.2272E-02		8.1722E-03
Fe	6.9844E-02		6.9844E-02	1.8747E-02
Ni	4.3063E-04		4.3063E-04	1.1559E-04
Cr	1.0385E-02		1.0385E-02	2.7875E-03
Mn55	4.6007E-04		4.6007E-04	1.2349E-04
Mo	4.9097E-04		4.9097E-04	1.3179E-04

10. Reflector

	Heterogeneous			Homogeneous
Nuclide	solid rod	Coolant	Duct	
Na		2.2272E-02		3.4976E-03
Fe	6.9844E-02		6.9844E-02	5.8876E-02
Ni	4.3063E-04		4.3063E-04	3.6301E-04
Cr	1.0385E-02		1.0385E-02	8.7541E-03
Mn55	4.6007E-04		4.6007E-04	3.8782E-04
Mo	4.9097E-04		4.9097E-04	4.1387E-04

11. Shield

	Heterogeneous				Homogeneous
Nuclide	Absorber	Clad	Coolant	Duct	
C	3.7154E-03				1.9422E-03
B10	1.5668E-02				8.1900E-03
B11	6.3065E-02				3.2966E-02
Na			2.2272E-02		3.8576E-03
Fe		6.9844E-02		6.9844E-02	2.1237E-02
Ni		4.3063E-04		4.3063E-04	1.3094E-04
Cr		1.0385E-02		1.0385E-02	3.1577E-03
Mn55		4.6007E-04		4.6007E-04	1.3989E-04
Mo		4.9097E-04		4.9097E-04	1.4929E-04

12. Outside core

	Heterogeneous		Homogeneous
	Barrel	Coolant	
Na		2.22724E-02	1.81469E-02
Fe	5.20478E-02		9.64075E-03
Ni	1.06872E-02		1.97959E-03
Cr	1.06058E-02		1.96450E-03
Mn55	1.66670E-03		3.08720E-04
Mo	1.42668E-03		2.64263E-04

APPENDIX B

15-GROUP CROSS SECTION LIBRARY

Each unique material in the core is given its own set of cross sections, presented in the following order:

$$\{\sigma_{cg}\}_{g=1}^{G}, \{\sigma_{fg}\}_{g=1}^{G}, \{v_g\}_{g=1}^{G}, \{\chi_g\}_{g=1}^{G}, \left\{\left\{\left\{\sigma_{sn}^{g'\to g}\right\}_{g'=1}^{G}\right\}_{g=1}^{G}\right\}_{n=0}^{N}$$

For G energy groups: σ_{cg} is the group g capture cross section, σ_{fg} is the group g fission cross section, v_g is the group g Nu bar, χ_g is the fission spectrum corresponding to group g, and finally $\sigma_{sn}^{g'\to g}$ represents the nth (out of N) Legendre moment of the scattering cross section for group g' to g.

Inner Core Fuel

1.1364E-01	1.4121E-01	1.5570E-01	1.8437E-01	2.6689E-01	3.3619E-01
3.7332E-01	3.9819E-01	4.3050E-01	4.1774E-01	4.9952E-01	5.7196E-01
3.9393E-01	2.9222E+00	2.8447E-01	2.6229E-02	1.8146E-02	1.6010E-02
6.5054E-03	5.5172E-03	5.4387E-03	5.6319E-03	6.1375E-03	8.2530E-03
1.8885E-02	4.8395E-02	1.1828E-01	5.1185E-02	1.6071E+00	1.0000E-15
3.6467E+00	3.0237E+00	2.8579E+00	2.9683E+00	2.9189E+00	2.8950E+00
2.8904E+00	2.8888E+00	2.8879E+00	2.8849E+00	2.8682E+00	2.8596E+00
2.8730E+00	2.8613E+00	1.0000E+00	2.2830E-02	3.0748E-01	2.3078E-01
3.0030E-01	1.0330E-01	2.6957E-02	6.4161E-03	1.4952E-03	3.8631E-04
4.4319E-05	5.9674E-06	1.3746E-07	0.0000E+00	0.0000E+00	0.0000E+00
1.0700E+02	1.8848E-02	2.6638E-02	1.3248E-02	1.8445E-02	7.6373E-03
1.9798E-03	4.3799E-04	9.1363E-05	1.4639E-05	3.0488E-06	0.0000E+00
0.0000E+00	0.0000E+00	0.0000E+00	0.0000E+00	0.0000E+00	6.0571E-02
2.6141E-02	2.2598E-02	1.0391E-02	2.4383E-03	4.1010E-04	7.2325E-05
1.8870E-05	2.8916E-06	6.2525E-07	7.4062E-08	0.0000E+00	0.0000E+00
0.0000E+00	0.0000E+00	0.0000E+00	8.0703E-02	4.3993E-02	1.0790E-02
2.2420E-03	4.3788E-04	8.2442E-05	1.8315E-05	1.4672E-06	5.7095E-07
0.0000E+00	0.0000E+00	0.0000E+00	0.0000E+00	0.0000E+00	0.0000E+00
0.0000E+00	1.5194E-01	2.0107E-02	2.4603E-03	4.5411E-04	1.4810E-04
5.7196E-05	2.7911E-06	2.3040E-07	0.0000E+00	0.0000E+00	0.0000E+00
0.0000E+00	0.0000E+00	0.0000E+00	0.0000E+00	0.0000E+00	2.4454E-01
1.3662E-02	4.8396E-05	6.6950E-06	1.1284E-06	9.4236E-08	0.0000E+00

0.0000E+00	0.0000E+00	0.0000E+00	0.0000E+00	0.0000E+00	0.0000E+00
0.0000E+00	0.0000E+00	0.0000E+00	3.1332E-01	1.2802E-02	9.9153E-05
1.1969E-06	8.4323E-08	0.0000E+00	0.0000E+00	0.0000E+00	0.0000E+00
0.0000E+00	0.0000E+00	0.0000E+00	0.0000E+00	0.0000E+00	0.0000E+00
0.0000E+00	3.4551E-01	1.3190E-02	5.0683E-05	4.3594E-06	2.5723E-07
0.0000E+00	0.0000E+00	0.0000E+00	0.0000E+00	0.0000E+00	0.0000E+00
0.0000E+00	0.0000E+00	0.0000E+00	0.0000E+00	0.0000E+00	3.6453E-01
1.3482E-02	3.1019E-05	1.5344E-06	0.0000E+00	0.0000E+00	0.0000E+00
0.0000E+00	0.0000E+00	0.0000E+00	0.0000E+00	0.0000E+00	0.0000E+00
0.0000E+00	0.0000E+00	0.0000E+00	3.8837E-01	1.1559E-02	8.2796E-07
0.0000E+00	0.0000E+00	0.0000E+00	0.0000E+00	0.0000E+00	0.0000E+00
0.0000E+00	0.0000E+00	0.0000E+00	0.0000E+00	0.0000E+00	0.0000E+00
0.0000E+00	3.5787E-01	6.9523E-03	0.0000E+00	0.0000E+00	0.0000E+00
0.0000E+00	0.0000E+00	0.0000E+00	0.0000E+00	0.0000E+00	0.0000E+00
0.0000E+00	0.0000E+00	0.0000E+00	0.0000E+00	0.0000E+00	3.7868E-01
2.3388E-03	0.0000E+00	0.0000E+00	0.0000E+00	0.0000E+00	0.0000E+00
0.0000E+00	0.0000E+00	0.0000E+00	0.0000E+00	0.0000E+00	0.0000E+00
0.0000E+00	0.0000E+00	0.0000E+00	2.7952E-01	3.7623E-03	0.0000E+00
0.0000E+00	0.0000E+00	0.0000E+00	0.0000E+00	0.0000E+00	0.0000E+00
0.0000E+00	0.0000E+00	0.0000E+00	0.0000E+00	0.0000E+00	0.0000E+00
1.5633E-04	2.7114E-01	1.5730E-03	0.0000E+00	0.0000E+00	0.0000E+00
0.0000E+00	0.0000E+00	0.0000E+00	0.0000E+00	0.0000E+00	0.0000E+00
0.0000E+00	0.0000E+00	0.0000E+00	0.0000E+00	5.1834E-03	2.7445E-01
8.9517E-04	0.0000E+00	0.0000E+00	0.0000E+00	0.0000E+00	0.0000E+00
0.0000E+00	0.0000E+00	0.0000E+00	0.0000E+00	0.0000E+00	0.0000E+00
0.0000E+00	0.0000E+00	2.1880E-05	2.1634E-04		

Test Site Fuel_____

1.1365E-01	1.4104E-01	1.5556E-01	1.8391E-01	2.6602E-01	3.3516E-01
3.7246E-01	3.9761E-01	4.3112E-01	4.2193E-01	5.1112E-01	6.2387E-01
5.4927E-01	2.5829E+00	2.7859E-01	2.6950E-02	1.8580E-02	1.6467E-02
6.4599E-03	4.4859E-03	4.3945E-03	4.6400E-03	5.2006E-03	7.2246E-03
1.6010E-02	4.2826E-02	1.3354E-01	4.6639E-02	1.1615E+00	1.0000E-15
3.6696E+00	3.0417E+00	2.8707E+00	2.9648E+00	2.9198E+00	2.9010E+00
2.8972E+00	2.8973E+00	2.8984E+00	2.8943E+00	2.8820E+00	2.8855E+00
2.9060E+00	2.8658E+00	1.0000E+00	2.2820E-02	3.0766E-01	2.3083E-01
3.0021E-01	1.0321E-01	2.6930E-02	6.4199E-03	1.4870E-03	3.8693E-04
4.2774E-05	6.0290E-06	4.5674E-08	2.2837E-08	0.0000E+00	0.0000E+00
1.0700E+02	1.8389E-02	2.6689E-02	1.3263E-02	1.8436E-02	7.3038E-03
1.9830E-03	4.2599E-04	9.6797E-05	2.4410E-05	1.2702E-05	0.0000E+00
0.0000E+00	0.0000E+00	0.0000E+00	0.0000E+00	0.0000E+00	6.0281E-02
2.5942E-02	2.2544E-02	1.0291E-02	2.4267E-03	4.2111E-04	7.7812E-05
1.8170E-05	2.2958E-06	6.9939E-07	1.9456E-07	8.6627E-08	0.0000E+00
0.0000E+00	0.0000E+00	0.0000E+00	8.0475E-02	4.3672E-02	1.0675E-02
2.2226E-03	4.3872E-04	7.7917E-05	1.8486E-05	1.2232E-06	5.8753E-07
0.0000E+00	0.0000E+00	0.0000E+00	0.0000E+00	0.0000E+00	0.0000E+00
0.0000E+00	1.5147E-01	2.0004E-02	2.4471E-03	4.5618E-04	1.4774E-04
5.5536E-05	2.6812E-06	2.0220E-07	0.0000E+00	0.0000E+00	0.0000E+00
0.0000E+00	0.0000E+00	0.0000E+00	0.0000E+00	0.0000E+00	2.4442E-01
1.3644E-02	4.8137E-05	7.3606E-06	1.2632E-06	4.8217E-08	0.0000E+00
0.0000E+00	0.0000E+00	0.0000E+00	0.0000E+00	0.0000E+00	0.0000E+00
0.0000E+00	0.0000E+00	0.0000E+00	3.1275E-01	1.2786E-02	9.6866E-05
1.2630E-06	6.4261E-08	0.0000E+00	0.0000E+00	0.0000E+00	0.0000E+00
0.0000E+00	0.0000E+00	0.0000E+00	0.0000E+00	0.0000E+00	0.0000E+00
0.0000E+00	3.4476E-01	1.3167E-02	5.1659E-05	4.2021E-06	2.5438E-07

0.0000E+00	0.0000E+00	0.0000E+00	0.0000E+00	0.0000E+00	0.0000E+00
0.0000E+00	0.0000E+00	0.0000E+00	0.0000E+00	0.0000E+00	3.6380E-01
1.3461E-02	3.2674E-05	1.4195E-06	0.0000E+00	0.0000E+00	0.0000E+00
0.0000E+00	0.0000E+00	0.0000E+00	0.0000E+00	0.0000E+00	0.0000E+00
0.0000E+00	0.0000E+00	0.0000E+00	3.8866E-01	1.1563E-02	1.0803E-06
0.0000E+00	0.0000E+00	0.0000E+00	0.0000E+00	0.0000E+00	0.0000E+00
0.0000E+00	0.0000E+00	0.0000E+00	0.0000E+00	0.0000E+00	0.0000E+00
0.0000E+00	3.6175E-01	7.0305E-03	0.0000E+00	0.0000E+00	0.0000E+00
0.0000E+00	0.0000E+00	0.0000E+00	0.0000E+00	0.0000E+00	0.0000E+00
0.0000E+00	0.0000E+00	0.0000E+00	0.0000E+00	0.0000E+00	3.8295E-01
2.3670E-03	0.0000E+00	0.0000E+00	0.0000E+00	0.0000E+00	0.0000E+00
0.0000E+00	0.0000E+00	0.0000E+00	0.0000E+00	0.0000E+00	0.0000E+00
0.0000E+00	0.0000E+00	0.0000E+00	2.8089E-01	3.7809E-03	0.0000E+00
0.0000E+00	0.0000E+00	0.0000E+00	0.0000E+00	0.0000E+00	0.0000E+00
0.0000E+00	0.0000E+00	0.0000E+00	0.0000E+00	0.0000E+00	0.0000E+00
1.7596E-04	2.8513E-01	1.6311E-03	0.0000E+00	0.0000E+00	0.0000E+00
0.0000E+00	0.0000E+00	0.0000E+00	0.0000E+00	0.0000E+00	0.0000E+00
0.0000E+00	0.0000E+00	0.0000E+00	0.0000E+00	4.9370E-03	2.6842E-01
9.1038E-04	0.0000E+00	0.0000E+00	0.0000E+00	0.0000E+00	0.0000E+00
0.0000E+00	0.0000E+00	0.0000E+00	0.0000E+00	0.0000E+00	0.0000E+00
0.0000E+00	0.0000E+00	3.0963E-05	2.4245E-04		

Outer Core Fuel_____

1.1438E-01	1.4158E-01	1.5585E-01	1.8460E-01	2.6715E-01	3.3657E-01
3.7412E-01	4.0044E-01	4.3481E-01	4.2795E-01	5.1716E-01	5.7149E-01
4.0017E-01	3.6441E+00	2.8946E-01	2.7325E-02	1.9284E-02	1.7378E-02
7.9444E-03	6.7791E-03	6.6803E-03	6.9137E-03	7.5165E-03	1.0185E-02
2.3410E-02	6.0220E-02	1.2613E-01	5.9618E-02	2.0488E+00	1.0000E-15
3.6755E+00	3.0581E+00	2.8899E+00	2.9720E+00	2.9195E+00	2.8959E+00
2.8914E+00	2.8900E+00	2.8892E+00	2.8857E+00	2.8701E+00	2.8616E+00
2.8739E+00	2.8608E+00	1.0000E+00	2.2839E-02	3.0758E-01	2.3074E-01
3.0029E-01	1.0330E-01	2.6916E-02	6.4030E-03	1.4947E-03	3.8912E-04
4.4863E-05	5.9558E-06	7.1633E-08	3.0700E-08	0.0000E+00	0.0000E+00
1.0700E+02	1.8592E-02	2.6693E-02	1.3174E-02	1.8418E-02	7.4845E-03
2.0248E-03	4.5458E-04	1.1319E-04	2.9867E-05	5.8884E-06	9.7065E-07
0.0000E+00	0.0000E+00	0.0000E+00	0.0000E+00	0.0000E+00	6.0170E-02
2.5888E-02	2.2643E-02	1.0238E-02	2.4168E-03	4.2113E-04	8.3556E-05
1.8733E-05	1.9968E-06	4.8648E-07	0.0000E+00	0.0000E+00	0.0000E+00
0.0000E+00	0.0000E+00	0.0000E+00	7.9993E-02	4.3659E-02	1.0679E-02
2.2296E-03	4.3241E-04	8.0679E-05	1.5944E-05	1.6693E-06	3.2679E-07
0.0000E+00	0.0000E+00	0.0000E+00	0.0000E+00	0.0000E+00	0.0000E+00
0.0000E+00	1.5098E-01	1.9932E-02	2.4360E-03	4.5581E-04	1.4543E-04
5.5648E-05	2.4436E-06	2.6718E-07	0.0000E+00	0.0000E+00	0.0000E+00
0.0000E+00	0.0000E+00	0.0000E+00	0.0000E+00	0.0000E+00	2.4356E-01
1.3596E-02	4.8519E-05	6.7614E-06	1.1226E-06	7.7104E-08	0.0000E+00
0.0000E+00	0.0000E+00	0.0000E+00	0.0000E+00	0.0000E+00	0.0000E+00
0.0000E+00	0.0000E+00	0.0000E+00	3.1241E-01	1.2779E-02	9.8425E-05
1.3162E-06	7.5560E-08	0.0000E+00	0.0000E+00	0.0000E+00	0.0000E+00
0.0000E+00	0.0000E+00	0.0000E+00	0.0000E+00	0.0000E+00	0.0000E+00
0.0000E+00	3.4495E-01	1.3190E-02	5.1590E-05	4.7379E-06	2.5535E-07
0.0000E+00	0.0000E+00	0.0000E+00	0.0000E+00	0.0000E+00	0.0000E+00
0.0000E+00	0.0000E+00	0.0000E+00	0.0000E+00	0.0000E+00	3.6509E-01
1.3528E-02	3.3224E-05	1.7083E-06	0.0000E+00	0.0000E+00	0.0000E+00
0.0000E+00	0.0000E+00	0.0000E+00	0.0000E+00	0.0000E+00	0.0000E+00
0.0000E+00	0.0000E+00	0.0000E+00	3.8939E-01	1.1581E-02	1.0213E-06

0.0000E+00	0.0000E+00	0.0000E+00	0.0000E+00	0.0000E+00	0.0000E+00
0.0000E+00	0.0000E+00	0.0000E+00	0.0000E+00	0.0000E+00	0.0000E+00
0.0000E+00	3.6034E-01	6.9828E-03	0.0000E+00	0.0000E+00	0.0000E+00
0.0000E+00	0.0000E+00	0.0000E+00	0.0000E+00	0.0000E+00	0.0000E+00
0.0000E+00	0.0000E+00	0.0000E+00	0.0000E+00	0.0000E+00	3.7740E-01
2.3362E-03	0.0000E+00	0.0000E+00	0.0000E+00	0.0000E+00	0.0000E+00
0.0000E+00	0.0000E+00	0.0000E+00	0.0000E+00	0.0000E+00	0.0000E+00
0.0000E+00	0.0000E+00	0.0000E+00	2.7620E-01	3.7259E-03	0.0000E+00
0.0000E+00	0.0000E+00	0.0000E+00	0.0000E+00	0.0000E+00	0.0000E+00
0.0000E+00	0.0000E+00	0.0000E+00	0.0000E+00	0.0000E+00	0.0000E+00
1.6786E-04	2.7091E-01	1.5490E-03	0.0000E+00	0.0000E+00	0.0000E+00
0.0000E+00	0.0000E+00	0.0000E+00	0.0000E+00	0.0000E+00	0.0000E+00
0.0000E+00	0.0000E+00	0.0000E+00	0.0000E+00	5.4638E-03	2.7928E-01
1.1606E-03	0.0000E+00	0.0000E+00	0.0000E+00	0.0000E+00	0.0000E+00
0.0000E+00	0.0000E+00	0.0000E+00	0.0000E+00	0.0000E+00	0.0000E+00
0.0000E+00	0.0000E+00	3.2998E-05	2.7263E-04		

Coolant (Sodium)

2.1229E-02	3.2869E-02	4.3210E-02	7.1999E-02	7.1858E-02	7.2324E-02
9.6859E-02	9.6621E-02	3.9467E-01	1.0925E-01	6.9784E-02	6.9605E-02
7.1431E-02	7.4535E-02	8.2528E-02	1.5584E-03	2.8172E-05	4.4597E-06
6.3686E-06	1.3868E-05	1.1545E-05	2.9394E-05	1.0939E-06	2.6536E-04
1.9397E-04	1.9283E-04	5.8985E-04	1.3548E-03	3.1810E-03	6.9893E-03
6.2000E+01	4.1300E-03	6.0792E-03	2.9798E-03	4.1811E-03	1.7216E-03
4.5929E-04	9.3152E-05	2.0135E-05	5.5478E-06	8.6137E-07	0.0000E+00
0.0000E+00	0.0000E+00	0.0000E+00	0.0000E+00	0.0000E+00	1.6228E-02
6.9758E-03	6.0728E-03	2.7767E-03	6.4983E-04	1.1276E-04	1.9856E-05
4.6741E-06	7.6555E-07	4.0109E-08	0.0000E+00	0.0000E+00	0.0000E+00
0.0000E+00	0.0000E+00	0.0000E+00	0.0000E+00	6.2456E-02	8.2579E-03
1.0076E-03	1.8711E-04	5.9853E-05	2.3168E-05	1.1184E-06	1.3298E-07
0.0000E+00	0.0000E+00	0.0000E+00	0.0000E+00	0.0000E+00	0.0000E+00
0.0000E+00	0.0000E+00	6.8030E-02	3.7993E-03	1.3321E-05	2.0303E-06
3.1671E-07	2.0288E-08	0.0000E+00	0.0000E+00	0.0000E+00	0.0000E+00
0.0000E+00	0.0000E+00	0.0000E+00	0.0000E+00	0.0000E+00	0.0000E+00
6.9454E-02	2.8368E-03	2.1714E-05	2.9352E-07	9.4883E-09	1.6145E-09
0.0000E+00	0.0000E+00	0.0000E+00	0.0000E+00	0.0000E+00	0.0000E+00
0.0000E+00	0.0000E+00	0.0000E+00	0.0000E+00	9.3252E-02	3.5623E-03
1.3926E-05	1.3059E-06	7.9111E-08	0.0000E+00	0.0000E+00	0.0000E+00
0.0000E+00	0.0000E+00	0.0000E+00	0.0000E+00	0.0000E+00	0.0000E+00
0.0000E+00	0.0000E+00	9.3166E-02	3.4460E-03	8.1818E-06	4.0179E-07
0.0000E+00	0.0000E+00	0.0000E+00	0.0000E+00	0.0000E+00	0.0000E+00
0.0000E+00	0.0000E+00	0.0000E+00	0.0000E+00	0.0000E+00	0.0000E+00
3.8301E-01	1.1398E-02	8.8570E-07	0.0000E+00	0.0000E+00	0.0000E+00
0.0000E+00	0.0000E+00	0.0000E+00	0.0000E+00	0.0000E+00	0.0000E+00
0.0000E+00	0.0000E+00	0.0000E+00	0.0000E+00	1.0698E-01	2.0775E-03
0.0000E+00	0.0000E+00	0.0000E+00	0.0000E+00	0.0000E+00	0.0000E+00
0.0000E+00	0.0000E+00	0.0000E+00	0.0000E+00	0.0000E+00	0.0000E+00
0.0000E+00	0.0000E+00	6.9163E-02	4.2767E-04	0.0000E+00	0.0000E+00
0.0000E+00	0.0000E+00	0.0000E+00	0.0000E+00	0.0000E+00	0.0000E+00
0.0000E+00	0.0000E+00	0.0000E+00	0.0000E+00	0.0000E+00	0.0000E+00
6.8100E-02	9.1464E-04	0.0000E+00	0.0000E+00	0.0000E+00	0.0000E+00
0.0000E+00	0.0000E+00	0.0000E+00	0.0000E+00	0.0000E+00	0.0000E+00
0.0000E+00	0.0000E+00	0.0000E+00	4.0032E-05	6.9649E-02	3.8692E-04
0.0000E+00	0.0000E+00	0.0000E+00	0.0000E+00	0.0000E+00	0.0000E+00

0.0000E+00	0.0000E+00	0.0000E+00	0.0000E+00	0.0000E+00	0.0000E+00
0.0000E+00	1.3249E-03	6.9750E-02	2.7909E-04	0.0000E+00	0.0000E+00
0.0000E+00	0.0000E+00	0.0000E+00	0.0000E+00	0.0000E+00	0.0000E+00
0.0000E+00	0.0000E+00	0.0000E+00	0.0000E+00	0.0000E+00	8.3401E-03
6.7199E-02	0.0000E+00	0.0000E+00	0.0000E+00	0.0000E+00	0.0000E+00
0.0000E+00	0.0000E+00	0.0000E+00	0.0000E+00	0.0000E+00	0.0000E+00
0.0000E+00	0.0000E+00	0.0000E+00	0.0000E+00	0.0000E+00	0.0000E+00
0.0000E+00	0.0000E+00	0.0000E+00	0.0000E+00	0.0000E+00	0.0000E+00
0.0000E+00	0.0000E+00	0.0000E+00	0.0000E+00	0.0000E+00	0.0000E+00
0.0000E+00	0.0000E+00	0.0000E+00	0.0000E+00	0.0000E+00	0.0000E+00
0.0000E+00	0.0000E+00	0.0000E+00	0.0000E+00	0.0000E+00	0.0000E+00
0.0000E+00	0.0000E+00	0.0000E+00	0.0000E+00		

Structural Components and Reflector

1.4937E-01	1.6969E-01	1.6855E-01	1.5963E-01	2.0853E-01	2.6103E-01
4.4793E-01	2.8600E-01	9.1898E-01	6.6109E-01	7.9524E-01	7.7904E-01
7.9505E-01	8.1902E-01	8.8959E-01	6.2756E-03	1.0730E-03	2.2003E-04
3.5029E-04	3.5843E-04	4.9534E-04	6.6374E-04	6.3449E-04	1.4437E-03
4.4175E-03	6.0099E-03	1.0487E-02	2.3793E-02	5.5536E-02	1.1691E-01
6.2000E+01	3.0043E-02	4.4223E-02	2.1677E-02	3.0415E-02	1.2524E-02
3.3411E-03	6.7763E-04	1.4647E-04	4.0357E-05	6.2660E-06	0.0000E+00
0.0000E+00	0.0000E+00	0.0000E+00	0.0000E+00	0.0000E+00	8.3319E-02
3.5817E-02	3.1181E-02	1.4257E-02	3.3365E-03	5.7898E-04	1.0195E-04
2.3999E-05	3.9307E-06	2.0594E-07	0.0000E+00	0.0000E+00	0.0000E+00
0.0000E+00	0.0000E+00	0.0000E+00	0.0000E+00	1.3818E-01	1.8270E-02
2.2291E-03	4.1396E-04	1.3242E-04	5.1258E-05	2.4744E-06	2.9421E-07
0.0000E+00	0.0000E+00	0.0000E+00	0.0000E+00	0.0000E+00	0.0000E+00
0.0000E+00	0.0000E+00	1.9712E-01	1.1008E-02	3.8597E-05	5.8829E-06
9.1766E-07	5.8785E-08	0.0000E+00	0.0000E+00	0.0000E+00	0.0000E+00
0.0000E+00	0.0000E+00	0.0000E+00	0.0000E+00	0.0000E+00	0.0000E+00
2.5023E-01	1.0221E-02	7.8231E-05	1.0575E-06	3.4185E-08	5.8167E-09
0.0000E+00	0.0000E+00	0.0000E+00	0.0000E+00	0.0000E+00	0.0000E+00
0.0000E+00	0.0000E+00	0.0000E+00	0.0000E+00	4.3075E-01	1.6455E-02
6.4324E-05	6.0321E-06	3.6542E-07	0.0000E+00	0.0000E+00	0.0000E+00
0.0000E+00	0.0000E+00	0.0000E+00	0.0000E+00	0.0000E+00	0.0000E+00
0.0000E+00	0.0000E+00	2.7516E-01	1.0178E-02	2.4165E-05	1.1867E-06
0.0000E+00	0.0000E+00	0.0000E+00	0.0000E+00	0.0000E+00	0.0000E+00
0.0000E+00	0.0000E+00	0.0000E+00	0.0000E+00	0.0000E+00	0.0000E+00
8.9102E-01	2.6516E-02	2.0605E-06	0.0000E+00	0.0000E+00	0.0000E+00
0.0000E+00	0.0000E+00	0.0000E+00	0.0000E+00	0.0000E+00	0.0000E+00
0.0000E+00	0.0000E+00	0.0000E+00	0.0000E+00	6.4416E-01	1.2510E-02
0.0000E+00	0.0000E+00	0.0000E+00	0.0000E+00	0.0000E+00	0.0000E+00
0.0000E+00	0.0000E+00	0.0000E+00	0.0000E+00	0.0000E+00	0.0000E+00
0.0000E+00	0.0000E+00	7.8438E-01	4.8502E-03	0.0000E+00	0.0000E+00
0.0000E+00	0.0000E+00	0.0000E+00	0.0000E+00	0.0000E+00	0.0000E+00
0.0000E+00	0.0000E+00	0.0000E+00	0.0000E+00	0.0000E+00	0.0000E+00
7.5837E-01	1.0186E-02	0.0000E+00	0.0000E+00	0.0000E+00	0.0000E+00
0.0000E+00	0.0000E+00	0.0000E+00	0.0000E+00	0.0000E+00	0.0000E+00
0.0000E+00	0.0000E+00	0.0000E+00	4.4059E-04	7.6656E-01	4.2584E-03
0.0000E+00	0.0000E+00	0.0000E+00	0.0000E+00	0.0000E+00	0.0000E+00
0.0000E+00	0.0000E+00	0.0000E+00	0.0000E+00	0.0000E+00	0.0000E+00
0.0000E+00	1.4177E-02	7.4633E-01	2.9863E-03	0.0000E+00	0.0000E+00
0.0000E+00	0.0000E+00	0.0000E+00	0.0000E+00	0.0000E+00	0.0000E+00
0.0000E+00	0.0000E+00	0.0000E+00	0.0000E+00	0.0000E+00	8.5310E-02

6.8737E-01	0.0000E+00	0.0000E+00	0.0000E+00	0.0000E+00	0.0000E+00
0.0000E+00	0.0000E+00	0.0000E+00	0.0000E+00	0.0000E+00	0.0000E+00
0.0000E+00	0.0000E+00	0.0000E+00	0.0000E+00	0.0000E+00	0.0000E+00
0.0000E+00	0.0000E+00	0.0000E+00	0.0000E+00	0.0000E+00	0.0000E+00
0.0000E+00	0.0000E+00	0.0000E+00	0.0000E+00	0.0000E+00	0.0000E+00
0.0000E+00	0.0000E+00	0.0000E+00	0.0000E+00	0.0000E+00	0.0000E+00
0.0000E+00	0.0000E+00	0.0000E+00	0.0000E+00	0.0000E+00	0.0000E+00
0.0000E+00	0.0000E+00	0.0000E+00	0.0000E+00		

Control Rod Absorber

7.1658E-02	9.9828E-02	1.4298E-01	1.6961E-01	3.1054E-01	3.6145E-01
4.0764E-01	4.5451E-01	4.9997E-01	6.5915E-01	1.0431E+00	3.2705E+00
6.8384E+00	1.5871E+01	3.7641E-01	5.8174E-03	6.6156E-03	7.1368E-03
6.8288E-03	1.8342E-02	3.1169E-02	4.7784E-02	7.6682E-02	1.3272E-01
2.9025E-01	6.7348E-01	2.9001E+00	6.4675E+00	1.5500E+01	1.0000E-15
6.2000E+01	1.3824E-02	2.0348E-02	9.9739E-03	1.3995E-02	5.7624E-03
1.5373E-03	3.1179E-04	6.7394E-05	1.8569E-05	2.8831E-06	0.0000E+00
0.0000E+00	0.0000E+00	0.0000E+00	0.0000E+00	0.0000E+00	4.6059E-02
1.9799E-02	1.7237E-02	7.8812E-03	1.8444E-03	3.2006E-04	5.6357E-05
1.3267E-05	2.1729E-06	1.1384E-07	0.0000E+00	0.0000E+00	0.0000E+00
0.0000E+00	0.0000E+00	0.0000E+00	0.0000E+00	1.4121E-01	1.8671E-02
2.2781E-03	4.2306E-04	1.3533E-04	5.2384E-05	2.5288E-06	3.0068E-07
0.0000E+00	0.0000E+00	0.0000E+00	0.0000E+00	0.0000E+00	0.0000E+00
0.0000E+00	0.0000E+00	2.7668E-01	1.5452E-02	5.4177E-05	8.2574E-06
1.2881E-06	8.2513E-08	0.0000E+00	0.0000E+00	0.0000E+00	0.0000E+00
0.0000E+00	0.0000E+00	0.0000E+00	0.0000E+00	0.0000E+00	0.0000E+00
3.1723E-01	1.2957E-02	9.9176E-05	1.3406E-06	4.3337E-08	7.3740E-09
0.0000E+00	0.0000E+00	0.0000E+00	0.0000E+00	0.0000E+00	0.0000E+00
0.0000E+00	0.0000E+00	0.0000E+00	0.0000E+00	3.4656E-01	1.3239E-02
5.1753E-05	4.8532E-06	2.9401E-07	0.0000E+00	0.0000E+00	0.0000E+00
0.0000E+00	0.0000E+00	0.0000E+00	0.0000E+00	0.0000E+00	0.0000E+00
0.0000E+00	0.0000E+00	3.6431E-01	1.3475E-02	3.1994E-05	1.5712E-06
0.0000E+00	0.0000E+00	0.0000E+00	0.0000E+00	0.0000E+00	0.0000E+00
0.0000E+00	0.0000E+00	0.0000E+00	0.0000E+00	0.0000E+00	0.0000E+00
3.5664E-01	1.0613E-02	8.2473E-07	0.0000E+00	0.0000E+00	0.0000E+00
0.0000E+00	0.0000E+00	0.0000E+00	0.0000E+00	0.0000E+00	0.0000E+00
0.0000E+00	0.0000E+00	0.0000E+00	0.0000E+00	3.6187E-01	7.0275E-03
0.0000E+00	0.0000E+00	0.0000E+00	0.0000E+00	0.0000E+00	0.0000E+00
0.0000E+00	0.0000E+00	0.0000E+00	0.0000E+00	0.0000E+00	0.0000E+00
0.0000E+00	0.0000E+00	3.6731E-01	2.2713E-03	0.0000E+00	0.0000E+00
0.0000E+00	0.0000E+00	0.0000E+00	0.0000E+00	0.0000E+00	0.0000E+00
0.0000E+00	0.0000E+00	0.0000E+00	0.0000E+00	0.0000E+00	0.0000E+00
3.6548E-01	4.9087E-03	0.0000E+00	0.0000E+00	0.0000E+00	0.0000E+00
0.0000E+00	0.0000E+00	0.0000E+00	0.0000E+00	0.0000E+00	0.0000E+00
0.0000E+00	0.0000E+00	0.0000E+00	2.1192E-04	3.6871E-01	2.0483E-03
0.0000E+00	0.0000E+00	0.0000E+00	0.0000E+00	0.0000E+00	0.0000E+00
0.0000E+00	0.0000E+00	0.0000E+00	0.0000E+00	0.0000E+00	0.0000E+00
0.0000E+00	6.8946E-03	3.6297E-01	1.4523E-03	0.0000E+00	0.0000E+00
0.0000E+00	0.0000E+00	0.0000E+00	0.0000E+00	0.0000E+00	0.0000E+00
0.0000E+00	0.0000E+00	0.0000E+00	0.0000E+00	0.0000E+00	7.3364E-05
5.9112E-04	0.0000E+00	0.0000E+00	0.0000E+00	0.0000E+00	0.0000E+00
0.0000E+00	0.0000E+00	0.0000E+00	0.0000E+00	0.0000E+00	0.0000E+00
0.0000E+00	0.0000E+00	0.0000E+00	0.0000E+00	0.0000E+00	0.0000E+00
0.0000E+00	0.0000E+00	0.0000E+00	0.0000E+00	0.0000E+00	0.0000E+00
0.0000E+00	0.0000E+00	0.0000E+00	0.0000E+00	0.0000E+00	0.0000E+00

0.0000E+00 0.0000E+00 0.0000E+00 0.0000E+00 0.0000E+00 0.0000E+00
0.0000E+00 0.0000E+00 0.0000E+00 0.0000E+00 0.0000E+00 0.0000E+00
0.0000E+00 0.0000E+00 0.0000E+00 0.0000E+00

Control Rod Lower Reflector

1.1393E-01 1.4077E-01 1.5463E-01 1.9112E-01 2.3184E-01 2.7640E-01
4.3205E-01 4.8287E-01 1.1108E+00 5.8519E-01 6.4071E-01 5.8442E-01
5.9783E-01 6.2451E-01 6.9834E-01 8.5685E-03 1.5196E-03 2.5004E-04
2.3926E-04 2.9678E-04 4.1745E-04 6.2295E-04 7.5313E-04 1.4181E-03
3.4357E-03 5.3359E-03 8.0391E-03 1.8321E-02 4.3395E-02 9.3101E-02
6.2000E+01 2.2122E-02 3.2564E-02 1.5962E-02 2.2396E-02 9.2217E-03
2.4602E-03 4.9897E-04 1.0785E-04 2.9717E-05 4.6139E-06 0.0000E+00
0.0000E+00 0.0000E+00 0.0000E+00 0.0000E+00 0.0000E+00 6.8805E-02
2.9578E-02 2.5749E-02 1.1773E-02 2.7553E-03 4.7813E-04 8.4189E-05
1.9818E-05 3.2460E-06 1.7007E-07 0.0000E+00 0.0000E+00 0.0000E+00
0.0000E+00 0.0000E+00 0.0000E+00 0.0000E+00 1.6559E-01 2.1894E-02
2.6714E-03 4.9609E-04 1.5869E-04 6.1427E-05 2.9653E-06 3.5258E-07
0.0000E+00 0.0000E+00 0.0000E+00 0.0000E+00 0.0000E+00 0.0000E+00
0.0000E+00 0.0000E+00 2.1925E-01 1.2244E-02 4.2931E-05 6.5434E-06
1.0207E-06 6.5386E-08 0.0000E+00 0.0000E+00 0.0000E+00 0.0000E+00
0.0000E+00 0.0000E+00 0.0000E+00 0.0000E+00 0.0000E+00 0.0000E+00
2.6507E-01 1.0827E-02 8.2869E-05 1.1202E-06 3.6212E-08 6.1615E-09
0.0000E+00 0.0000E+00 0.0000E+00 0.0000E+00 0.0000E+00 0.0000E+00
0.0000E+00 0.0000E+00 0.0000E+00 0.0000E+00 4.1549E-01 1.5872E-02
6.2046E-05 5.8185E-06 3.5248E-07 0.0000E+00 0.0000E+00 0.0000E+00
0.0000E+00 0.0000E+00 0.0000E+00 0.0000E+00 0.0000E+00 0.0000E+00
0.0000E+00 0.0000E+00 4.6488E-01 1.7195E-02 4.0826E-05 2.0049E-06
0.0000E+00 0.0000E+00 0.0000E+00 0.0000E+00 0.0000E+00 0.0000E+00
0.0000E+00 0.0000E+00 0.0000E+00 0.0000E+00 0.0000E+00 0.0000E+00
1.0773E+00 3.2059E-02 2.4912E-06 0.0000E+00 0.0000E+00 0.0000E+00
0.0000E+00 0.0000E+00 0.0000E+00 0.0000E+00 0.0000E+00 0.0000E+00
0.0000E+00 0.0000E+00 0.0000E+00 0.0000E+00 5.7067E-01 1.1082E-02
0.0000E+00 0.0000E+00 0.0000E+00 0.0000E+00 0.0000E+00 0.0000E+00
0.0000E+00 0.0000E+00 0.0000E+00 0.0000E+00 0.0000E+00 0.0000E+00
0.0000E+00 0.0000E+00 6.3147E-01 3.9047E-03 0.0000E+00 0.0000E+00
0.0000E+00 0.0000E+00 0.0000E+00 0.0000E+00 0.0000E+00 0.0000E+00
0.0000E+00 0.0000E+00 0.0000E+00 0.0000E+00 0.0000E+00 0.0000E+00
5.6875E-01 7.6387E-03 0.0000E+00 0.0000E+00 0.0000E+00 0.0000E+00
0.0000E+00 0.0000E+00 0.0000E+00 0.0000E+00 0.0000E+00 0.0000E+00
0.0000E+00 0.0000E+00 0.0000E+00 3.3105E-04 5.7598E-01 3.1997E-03
0.0000E+00 0.0000E+00 0.0000E+00 0.0000E+00 0.0000E+00 0.0000E+00
0.0000E+00 0.0000E+00 0.0000E+00 0.0000E+00 0.0000E+00 0.0000E+00
0.0000E+00 1.0790E-02 5.6805E-01 2.2729E-03 0.0000E+00 0.0000E+00
0.0000E+00 0.0000E+00 0.0000E+00 0.0000E+00 0.0000E+00 0.0000E+00
0.0000E+00 0.0000E+00 0.0000E+00 0.0000E+00 0.0000E+00 6.6824E-02
5.3842E-01 0.0000E+00 0.0000E+00 0.0000E+00 0.0000E+00 0.0000E+00
0.0000E+00 0.0000E+00 0.0000E+00 0.0000E+00 0.0000E+00 0.0000E+00
0.0000E+00 0.0000E+00 0.0000E+00 0.0000E+00 0.0000E+00 0.0000E+00
0.0000E+00 0.0000E+00 0.0000E+00 0.0000E+00 0.0000E+00 0.0000E+00
0.0000E+00 0.0000E+00 0.0000E+00 0.0000E+00 0.0000E+00 0.0000E+00
0.0000E+00 0.0000E+00 0.0000E+00 0.0000E+00 0.0000E+00 0.0000E+00
0.0000E+00 0.0000E+00 0.0000E+00 0.0000E+00

APPENDIX C

SELECTED FISSION DENSITY DISTRIBUTIONS

The first set of tables contains the assembly mesh average pin fission densities. In these tables, the assembly numbering is identical to the previously defined numbering scheme and meshes 1 through 5 are the axial levels of the core. 1 is the bottom, 5 is the top.

Average Pin Fission Densities ARO

	1	2	3	4	5	6
5	0.849103	0.833853	0.72269	0.737216	0.759952	0.632123
4	1.272949	1.252278	1.079512	1.106148	1.149094	0.9478
3	1.477798	1.452252	1.250896	1.28278	1.334082	1.097927
2	1.438653	1.401154	1.212035	1.237415	1.285669	1.056313
1	1.438653	1.401154	1.212035	1.237415	1.285669	1.056313
	7	8	9	10	11	
5	0.709357	0.527714	0.70302	0.672487	0.52276	
4	1.043674	0.753704	1.033655	0.970994	0.746222	
3	1.206561	0.868082	1.194763	1.118479	0.859501	
2	1.168769	0.849698	1.158936	1.07697	0.842428	
1	1.168769	0.849698	1.158936	1.07697	0.842428	

Average Pin Fission Densities NC

	1	2	3	4	5	6
5	0.890533	0.83009	0.747908	0.757763	0.757066	0.634844
4	1.309379	1.221647	1.094018	1.111014	1.12108	0.93172
3	1.493811	1.392918	1.245137	1.265099	1.279507	1.060393
2	1.418786	1.317652	1.179422	1.193618	1.208208	0.998713
1	1.136087	1.038718	0.938886	0.934935	0.940617	0.772855
	7	8	9	10	11	
5	0.758249	0.602124	0.753066	0.686749	0.597697	
4	1.09245	0.847462	1.085063	0.971431	0.841288	
3	1.239084	0.956853	1.230746	1.09903	0.950135	
2	1.168047	0.90328	1.161669	1.034651	0.898129	
1	0.917195	0.718194	0.915129	0.81088	0.716062	

Average Pin Fission Densities ARI

	1	2	3	4	5	6
5	0.805662	0.812117	0.702037	0.781345	0.769196	0.670213
4	1.20687	1.219261	1.047182	1.171657	1.161862	1.003997
3	1.378768	1.392123	1.193839	1.336753	1.327629	1.144127
2	1.287118	1.298025	1.112506	1.245098	1.237799	1.06521
1	0.987145	0.98482	0.848376	0.939529	0.931799	0.798192
	7	8	9	10	11	
5	0.782549	0.594297	0.754246	0.740139	0.572048	
4	1.151022	0.84819	1.107037	1.068189	0.814574	
3	1.307884	0.958643	1.257264	1.209949	0.920158	
2	1.217862	0.893918	1.171405	1.128032	0.858622	
1	0.92342	0.689636	0.891141	0.85994	0.664338	

The second two tables contain the coordinates and normalized pin fission density results for two assembly meshes: the peak assembly mesh of the near critical configuration (Assembly 1, Mesh 3) and a high leakage assembly mesh of the near critical configuration (Assembly 9, Mesh 5).

Assembly 1 Mesh 3 Pin Fission Densities

x (cm)	y (cm)	z (cm)	Pin Fission Density
8.35678	17.54238	42.2	1.497118
8.35678	18.45578	42.2	1.500301
8.35678	19.36918	42.2	1.500185
8.35678	20.28258	42.2	1.498469
8.35678	21.19598	42.2	1.49302
8.35678	22.10938	42.2	1.487894
8.35678	23.02278	42.2	1.481328
8.35678	23.93618	42.2	1.470851
8.35678	24.84958	42.2	1.452698
9.14781	17.08568	42.2	1.50004
9.14781	17.99908	42.2	1.507617
9.14781	18.91248	42.2	1.505389
9.14781	19.82588	42.2	1.507095
9.14781	20.73928	42.2	1.50412
9.14781	21.65268	42.2	1.500286
9.14781	22.56608	42.2	1.491968
9.14781	23.47948	42.2	1.48118
9.14781	24.39288	42.2	1.468348

Assembly 1 Mesh 3 Pin Fission Densities

x (cm)	y (cm)	z (cm)	Pin Fission Density
14.68501	21.19598	42.2	1.51744
14.68501	22.10938	42.2	1.510489
14.68501	23.02278	42.2	1.505826
14.68501	23.93618	42.2	1.497096
14.68501	24.84958	42.2	1.487658
14.68501	25.76298	42.2	1.476023
14.68501	26.67638	42.2	1.462458
14.68501	27.58978	42.2	1.448423
14.68501	28.50318	42.2	1.431518
15.47604	14.34548	42.2	1.510504
15.47604	15.25888	42.2	1.516996
15.47604	16.17228	42.2	1.523283
15.47604	17.08568	42.2	1.526755
15.47604	17.99908	42.2	1.524633
15.47604	18.91248	42.2	1.524948
15.47604	19.82588	42.2	1.523692
15.47604	20.73928	42.2	1.521381
15.47604	21.65268	42.2	1.514767

9.14781	25.30628	42.2	1.447032
9.93884	16.62898	42.2	1.499048
9.93884	17.54238	42.2	1.510788
9.93884	18.45578	42.2	1.512422
9.93884	19.36918	42.2	1.514326
9.93884	20.28258	42.2	1.509761
9.93884	21.19598	42.2	1.505974
9.93884	22.10938	42.2	1.499725
9.93884	23.02278	42.2	1.488064
9.93884	23.93618	42.2	1.477597
9.93884	24.84958	42.2	1.465074
9.93884	25.76298	42.2	1.444885
10.72987	16.17228	42.2	1.50474
10.72987	17.08568	42.2	1.509824
10.72987	17.99908	42.2	1.514754
10.72987	18.91248	42.2	1.512856
10.72987	19.82588	42.2	1.513734
10.72987	20.73928	42.2	1.509884
10.72987	21.65268	42.2	1.505845
10.72987	22.56608	42.2	1.497008
10.72987	23.47948	42.2	1.488804
10.72987	24.39288	42.2	1.47516
10.72987	25.30628	42.2	1.461787
10.72987	26.21968	42.2	1.44389
11.52089	15.71558	42.2	1.505121
11.52089	16.62898	42.2	1.513064
11.52089	17.54238	42.2	1.515091
11.52089	18.45578	42.2	1.516694
11.52089	19.36918	42.2	1.520811
11.52089	20.28258	42.2	1.513618
11.52089	21.19598	42.2	1.51403
11.52089	22.10938	42.2	1.502996
11.52089	23.02278	42.2	1.495176
11.52089	23.93618	42.2	1.488064
11.52089	24.84958	42.2	1.476939
11.52089	25.76298	42.2	1.461705
11.52089	26.67638	42.2	1.439162
12.31192	15.25888	42.2	1.505005
12.31192	16.17228	42.2	1.514704
12.31192	17.08568	42.2	1.516306
12.31192	17.99908	42.2	1.52179
12.31192	18.91248	42.2	1.521686
12.31192	19.82588	42.2	1.52027
15.47604	22.56608	42.2	1.507882
15.47604	23.47948	42.2	1.502562
15.47604	24.39288	42.2	1.49421
15.47604	25.30628	42.2	1.481104
15.47604	26.21968	42.2	1.471817
15.47604	27.13308	42.2	1.462004
15.47604	28.04648	42.2	1.443153
16.26707	14.80218	42.2	1.514811
16.26707	15.71558	42.2	1.523081
16.26707	16.62898	42.2	1.522804
16.26707	17.54238	42.2	1.525987
16.26707	18.45578	42.2	1.525433
16.26707	19.36918	42.2	1.524728
16.26707	20.28258	42.2	1.523912
16.26707	21.19598	42.2	1.520799
16.26707	22.10938	42.2	1.511134
16.26707	23.02278	42.2	1.504381
16.26707	23.93618	42.2	1.497386
16.26707	24.84958	42.2	1.490567
16.26707	25.76298	42.2	1.480814
16.26707	26.67638	42.2	1.467161
16.26707	27.58978	42.2	1.453659
17.0581	15.25888	42.2	1.516171
17.0581	16.17228	42.2	1.522508
17.0581	17.08568	42.2	1.52452
17.0581	17.99908	42.2	1.526409
17.0581	18.91248	42.2	1.522851
17.0581	19.82588	42.2	1.525068
17.0581	20.73928	42.2	1.51958
17.0581	21.65268	42.2	1.515006
17.0581	22.56608	42.2	1.509522
17.0581	23.47948	42.2	1.503292
17.0581	24.39288	42.2	1.494688
17.0581	25.30628	42.2	1.485662
17.0581	26.21968	42.2	1.476218
17.0581	27.13308	42.2	1.460522
17.84913	15.71558	42.2	1.517729
17.84913	16.62898	42.2	1.520559
17.84913	17.54238	42.2	1.524142
17.84913	18.45578	42.2	1.520666
17.84913	19.36918	42.2	1.521608
17.84913	20.28258	42.2	1.517481
17.84913	21.19598	42.2	1.515828

12.31192	20.73928	42.2	1.514358
12.31192	21.65268	42.2	1.511691
12.31192	22.56608	42.2	1.505266
12.31192	23.47948	42.2	1.495173
12.31192	24.39288	42.2	1.48462
12.31192	25.30628	42.2	1.473155
12.31192	26.21968	42.2	1.456583
12.31192	27.13308	42.2	1.435765
13.10295	14.80218	42.2	1.504668
13.10295	15.71558	42.2	1.512746
13.10295	16.62898	42.2	1.519753
13.10295	17.54238	42.2	1.522895
13.10295	18.45578	42.2	1.523153
13.10295	19.36918	42.2	1.524214
13.10295	20.28258	42.2	1.519278
13.10295	21.19598	42.2	1.514011
13.10295	22.10938	42.2	1.510457
13.10295	23.02278	42.2	1.503273
13.10295	23.93618	42.2	1.490183
13.10295	24.84958	42.2	1.481472
13.10295	25.76298	42.2	1.467939
13.10295	26.67638	42.2	1.455645
13.10295	27.58978	42.2	1.437358
13.89398	14.34548	42.2	1.503374
13.89398	15.25888	42.2	1.513341
13.89398	16.17228	42.2	1.520836
13.89398	17.08568	42.2	1.523138
13.89398	17.99908	42.2	1.525105
13.89398	18.91248	42.2	1.52616
13.89398	19.82588	42.2	1.521051
13.89398	20.73928	42.2	1.517761
13.89398	21.65268	42.2	1.512211
13.89398	22.56608	42.2	1.508745
13.89398	23.47948	42.2	1.500925
13.89398	24.39288	42.2	1.492343
13.89398	25.30628	42.2	1.479939
13.89398	26.21968	42.2	1.466431
13.89398	27.13308	42.2	1.455636
13.89398	28.04648	42.2	1.435129
14.68501	13.88878	42.2	1.505086
14.68501	14.80218	42.2	1.514251
14.68501	15.71558	42.2	1.519662
14.68501	16.62898	42.2	1.526472
17.84913	22.10938	42.2	1.510328
17.84913	23.02278	42.2	1.503295
17.84913	23.93618	42.2	1.497458
17.84913	24.84958	42.2	1.490171
17.84913	25.76298	42.2	1.480493
17.84913	26.67638	42.2	1.465193
18.64016	16.17228	42.2	1.515274
18.64016	17.08568	42.2	1.520616
18.64016	17.99908	42.2	1.519949
18.64016	18.91248	42.2	1.519798
18.64016	19.82588	42.2	1.513974
18.64016	20.73928	42.2	1.513986
18.64016	21.65268	42.2	1.511682
18.64016	22.56608	42.2	1.502895
18.64016	23.47948	42.2	1.496671
18.64016	24.39288	42.2	1.490136
18.64016	25.30628	42.2	1.481312
18.64016	26.21968	42.2	1.469768
19.43119	16.62898	42.2	1.512736
19.43119	17.54238	42.2	1.517358
19.43119	18.45578	42.2	1.512544
19.43119	19.36918	42.2	1.513835
19.43119	20.28258	42.2	1.51115
19.43119	21.19598	42.2	1.504567
19.43119	22.10938	42.2	1.50236
19.43119	23.02278	42.2	1.497531
19.43119	23.93618	42.2	1.488464
19.43119	24.84958	42.2	1.47873
19.43119	25.76298	42.2	1.46899
20.22222	17.08568	42.2	1.505713
20.22222	17.99908	42.2	1.510309
20.22222	18.91248	42.2	1.510133
20.22222	19.82588	42.2	1.506994
20.22222	20.73928	42.2	1.501305
20.22222	21.65268	42.2	1.499143
20.22222	22.56608	42.2	1.492966
20.22222	23.47948	42.2	1.484617
20.22222	24.39288	42.2	1.478604
20.22222	25.30628	42.2	1.4699
21.01325	17.54238	42.2	1.501639
21.01325	18.45578	42.2	1.500673
21.01325	19.36918	42.2	1.500241
21.01325	20.28258	42.2	1.497821

14.68501	17.54238	42.2	1.526922
14.68501	18.45578	42.2	1.525272
14.68501	19.36918	42.2	1.525823
14.68501	20.28258	42.2	1.522603

21.01325	21.19598	42.2	1.489075
21.01325	22.10938	42.2	1.488829
21.01325	23.02278	42.2	1.480676
21.01325	23.93618	42.2	1.475182
21.01325	24.84958	42.2	1.464293

Assembly 9 Mesh 5 Pin Fission Densities

x (cm)	y (cm)	z (cm)	Pin Fission Density
15.69928	55.6951	75.96	0.795159
15.69928	56.6085	75.96	0.787705
15.69928	57.5219	75.96	0.778817
15.69928	58.4353	75.96	0.76631
15.69928	59.3487	75.96	0.759016
15.69928	60.2621	75.96	0.748743
15.69928	61.1755	75.96	0.73855
15.69928	62.0889	75.96	0.726603
15.69928	63.0023	75.96	0.715336
16.49031	55.2384	75.96	0.805806
16.49031	56.1518	75.96	0.796091
16.49031	57.0652	75.96	0.787746
16.49031	57.9786	75.96	0.778984
16.49031	58.892	75.96	0.76885
16.49031	59.8054	75.96	0.75657
16.49031	60.7188	75.96	0.746845
16.49031	61.6322	75.96	0.734199
16.49031	62.5456	75.96	0.722243
16.49031	63.459	75.96	0.709518
17.28134	54.7817	75.96	0.812295
17.28134	55.6951	75.96	0.803694
17.28134	56.6085	75.96	0.796718
17.28134	57.5219	75.96	0.785797
17.28134	58.4353	75.96	0.774451
17.28134	59.3487	75.96	0.766197
17.28134	60.2621	75.96	0.751904
17.28134	61.1755	75.96	0.742838
17.28134	62.0889	75.96	0.730119
17.28134	63.0023	75.96	0.716437
17.28134	63.9157	75.96	0.704906
18.07237	54.325	75.96	0.820486

Assembly 9 Mesh 5 Pin Fission Densities

x (cm)	y (cm)	z (cm)	Pin Fission Density
22.02751	59.3487	75.96	0.762803
22.02751	60.2621	75.96	0.751407
22.02751	61.1755	75.96	0.738736
22.02751	62.0889	75.96	0.724815
22.02751	63.0023	75.96	0.710774
22.02751	63.9157	75.96	0.700908
22.02751	64.8291	75.96	0.688586
22.02751	65.7425	75.96	0.672395
22.02751	66.6559	75.96	0.662044
22.81854	52.4982	75.96	0.83147
22.81854	53.4116	75.96	0.82398
22.81854	54.325	75.96	0.815484
22.81854	55.2384	75.96	0.809231
22.81854	56.1518	75.96	0.798226
22.81854	57.0652	75.96	0.789118
22.81854	57.9786	75.96	0.778518
22.81854	58.892	75.96	0.768035
22.81854	59.8054	75.96	0.755194
22.81854	60.7188	75.96	0.741292
22.81854	61.6322	75.96	0.730528
22.81854	62.5456	75.96	0.715518
22.81854	63.459	75.96	0.701931
22.81854	64.3724	75.96	0.692294
22.81854	65.2858	75.96	0.679752
22.81854	66.1992	75.96	0.666788
23.60957	52.9549	75.96	0.822828
23.60957	53.8683	75.96	0.817136
23.60957	54.7817	75.96	0.809323
23.60957	55.6951	75.96	0.800319
23.60957	56.6085	75.96	0.792524
23.60957	57.5219	75.96	0.781594

18.07237	55.2384	75.96	0.811463	23.60957	58.4353	75.96	0.7688
18.07237	56.1518	75.96	0.802715	23.60957	59.3487	75.96	0.757779
18.07237	57.0652	75.96	0.792386	23.60957	60.2621	75.96	0.744323
18.07237	57.9786	75.96	0.782176	23.60957	61.1755	75.96	0.733406
18.07237	58.892	75.96	0.770865	23.60957	62.0889	75.96	0.720486
18.07237	59.8054	75.96	0.759941	23.60957	63.0023	75.96	0.707169
18.07237	60.7188	75.96	0.749335	23.60957	63.9157	75.96	0.696315
18.07237	61.6322	75.96	0.736066	23.60957	64.8291	75.96	0.684336
18.07237	62.5456	75.96	0.724956	23.60957	65.7425	75.96	0.67288
18.07237	63.459	75.96	0.712288	24.4006	53.4116	75.96	0.818012
18.07237	64.3724	75.96	0.696154	24.4006	54.325	75.96	0.808473
18.86339	53.8683	75.96	0.824434	24.4006	55.2384	75.96	0.801962
18.86339	54.7817	75.96	0.817288	24.4006	56.1518	75.96	0.793097
18.86339	55.6951	75.96	0.808133	24.4006	57.0652	75.96	0.781789
18.86339	56.6085	75.96	0.797561	24.4006	57.9786	75.96	0.771785
18.86339	57.5219	75.96	0.785847	24.4006	58.892	75.96	0.762343
18.86339	58.4353	75.96	0.777092	24.4006	59.8054	75.96	0.751136
18.86339	59.3487	75.96	0.767604	24.4006	60.7188	75.96	0.73781
18.86339	60.2621	75.96	0.755751	24.4006	61.6322	75.96	0.723628
18.86339	61.1755	75.96	0.742863	24.4006	62.5456	75.96	0.71339
18.86339	62.0889	75.96	0.730881	24.4006	63.459	75.96	0.699894
18.86339	63.0023	75.96	0.717889	24.4006	64.3724	75.96	0.689672
18.86339	63.9157	75.96	0.705605	24.4006	65.2858	75.96	0.675694
18.86339	64.8291	75.96	0.691825	25.19163	53.8683	75.96	0.807047
19.65442	53.4116	75.96	0.826609	25.19163	54.7817	75.96	0.801434
19.65442	54.325	75.96	0.82115	25.19163	55.6951	75.96	0.794297
19.65442	55.2384	75.96	0.812679	25.19163	56.6085	75.96	0.782982
19.65442	56.1518	75.96	0.804676	25.19163	57.5219	75.96	0.773588
19.65442	57.0652	75.96	0.79379	25.19163	58.4353	75.96	0.762866
19.65442	57.9786	75.96	0.783514	25.19163	59.3487	75.96	0.7509
19.65442	58.892	75.96	0.772357	25.19163	60.2621	75.96	0.739066
19.65442	59.8054	75.96	0.760794	25.19163	61.1755	75.96	0.729304
19.65442	60.7188	75.96	0.749877	25.19163	62.0889	75.96	0.714256
19.65442	61.6322	75.96	0.73435	25.19163	63.0023	75.96	0.705183
19.65442	62.5456	75.96	0.723546	25.19163	63.9157	75.96	0.692852
19.65442	63.459	75.96	0.710059	25.19163	64.8291	75.96	0.679947
19.65442	64.3724	75.96	0.697272	25.98266	54.325	75.96	0.801881
19.65442	65.2858	75.96	0.682277	25.98266	55.2384	75.96	0.792232
20.44545	52.9549	75.96	0.833041	25.98266	56.1518	75.96	0.785473
20.44545	53.8683	75.96	0.825624	25.98266	57.0652	75.96	0.77453
20.44545	54.7817	75.96	0.818496	25.98266	57.9786	75.96	0.766178
20.44545	55.6951	75.96	0.8075	25.98266	58.892	75.96	0.754775
20.44545	56.6085	75.96	0.800618	25.98266	59.8054	75.96	0.742324

20.44545	57.5219	75.96	0.789099
20.44545	58.4353	75.96	0.779145
20.44545	59.3487	75.96	0.76495
20.44545	60.2621	75.96	0.75282
20.44545	61.1755	75.96	0.740895
20.44545	62.0889	75.96	0.729556
20.44545	63.0023	75.96	0.715751
20.44545	63.9157	75.96	0.704084
20.44545	64.8291	75.96	0.68846
20.44545	65.7425	75.96	0.674051
21.23648	52.4982	75.96	0.834687
21.23648	53.4116	75.96	0.82778
21.23648	54.325	75.96	0.820225
21.23648	55.2384	75.96	0.81146
21.23648	56.1518	75.96	0.803304
21.23648	57.0652	75.96	0.792723
21.23648	57.9786	75.96	0.782346
21.23648	58.892	75.96	0.769386
21.23648	59.8054	75.96	0.756667
21.23648	60.7188	75.96	0.746231
21.23648	61.6322	75.96	0.732889
21.23648	62.5456	75.96	0.719907
21.23648	63.459	75.96	0.709546
21.23648	64.3724	75.96	0.693695
21.23648	65.2858	75.96	0.681562
21.23648	66.1992	75.96	0.668246
22.02751	52.0415	75.96	0.836438
22.02751	52.9549	75.96	0.830305
22.02751	53.8683	75.96	0.826313
22.02751	54.7817	75.96	0.815323
22.02751	55.6951	75.96	0.80643
22.02751	56.6085	75.96	0.79701
22.02751	57.5219	75.96	0.78387
22.02751	58.4353	75.96	0.774029
25.98266	60.7188	75.96	0.728699
25.98266	61.6322	75.96	0.718181
25.98266	62.5456	75.96	0.70789
25.98266	63.459	75.96	0.694297
25.98266	64.3724	75.96	0.683996
26.77369	54.7817	75.96	0.792581
26.77369	55.6951	75.96	0.786071
26.77369	56.6085	75.96	0.775185
26.77369	57.5219	75.96	0.764818
26.77369	58.4353	75.96	0.758125
26.77369	59.3487	75.96	0.743735
26.77369	60.2621	75.96	0.730692
26.77369	61.1755	75.96	0.719598
26.77369	62.0889	75.96	0.709049
26.77369	63.0023	75.96	0.69674
26.77369	63.9157	75.96	0.687686
27.56472	55.2384	75.96	0.782029
27.56472	56.1518	75.96	0.773667
27.56472	57.0652	75.96	0.765813
27.56472	57.9786	75.96	0.755858
27.56472	58.892	75.96	0.743653
27.56472	59.8054	75.96	0.732723
27.56472	60.7188	75.96	0.723451
27.56472	61.6322	75.96	0.709971
27.56472	62.5456	75.96	0.699075
27.56472	63.459	75.96	0.687198
28.35575	55.6951	75.96	0.771649
28.35575	56.6085	75.96	0.762856
28.35575	57.5219	75.96	0.755635
28.35575	58.4353	75.96	0.743193
28.35575	59.3487	75.96	0.732594
28.35575	60.2621	75.96	0.721563
28.35575	61.1755	75.96	0.710314
28.35575	62.0889	75.96	0.700939
28.35575	63.0023	75.96	0.689178

REFERENCES

[1] Cahalan et al, "Advanced Burner Test Reactor Preconceptual Design Report," Argonne National Laboratory, Argonne, IL, 2008.

[2] ANL-NED, "Benchmark of Advanced Burner Test Reactor," Argonne National Laboratory, Argonne, IL, 2009.

[3] Allen, K., Knight, T., Bays, S., "Benchmark of Advanced Burner Test Reactor using MCNPX 2.6.0 and ERANOS 2.1," *Prog. Nucl. Energy*, vol. 53, no. 6, pp. 633–644, 2010.

[4] Pounders, J., Rahnema, F. , Stamm'ler, R., "Stochastically Generated Multigroup Cross Sections," Georgia Institute of Technology, GA, 2006.

[5] Aliberti, G., Palmiotti, G., Salvatores, M., Stenberg, C. G., "Impact of Nuclear Data Uncertainties on Transmutation of Actinides in Accelerator-Driven Assemblies," *Nucl. Sci. Eng.*, vol 146, pp. 13–50, 2004.

[6] Connolly, K.J., Rahnema, "A heterogeneous coarse mesh radiation transport method for neutronic analysis of prismatic reactors," *Ann. Nucl. Energy*, vol 56, pp. 87–101, 2013.

[7] Connolly, K.J. et al, "A coarse mesh radiation transport method for 2-D hexagonal geometry," *Ann. Nucl. Energy*, vol. 42, pp. 1–10, 2012.

[8] X-5 Monte Carlo Team, "MCNP—A General Monte Carlo N-Particle Transport Code, Version 5," Los Alamos National Laboratory, 2005.

[9] Mosher, S.W., Rahnema, F., "The incident flux response expansion method for heterogeneous coarse mesh transport problems," *Trans. Theory Stat. Phys.*, vol. 35, pp. 55–86, 2006.

[10] Zhang, D., Rahnema, F., "An efficient hybrid stochastic/deterministic coarse mesh neutron transport method," *Ann. Nucl. Energy*, vol. 41, pp. 1–11, 2012.

[11] Stamm'ler, R.J.J., Abbate, M.J., "Methods of Steady-State Reactor Physics in Nuclear Design," Academic Press, London, 1983.